A STUDY OF ALKANEDITHIOL FUNCTIONALIZED ZINC PHOSPHIDE NANOWIRES FOR SOLAR HYDROGEN PRODUCTION

A Thesis

by

HAI LI

Submitted to the Office of Graduate and Professional Studies of
Texas A&M University
in partial fulfillment of the requirements for the degree of

MASTER OF SCIENCE

Chair of Committee,	Zhengdong Cheng
Committee Members,	Perla Beatriz Balbuena
	Ying Li
Head of Department,	M. Nazmul Karim

May 2016

Major Subject: Chemical Engineering

ABSTRACT

Structure stability and photocatalytic activity were investigated for the un-functionalized Zn_3P_2 nanowires and the functionalized Zn_3P_2 nanowires using photocatalytic hydrogen evolution and SEM characterization. The dependence of alkyne chain length in alkanedithiol functional groups with photocatalytic activity of the functionalized Zn_3P_2 nanowires was demonstrated by photocatalytic hydrogen evolution. Metal-doped Ag/Zn_3P_2 nanowires nanocomposite was evaluated and characterized by photocatalytic hydrogen evolution, EDX, SEM.

The functionalized Zn_3P_2 nanowires exhibit better nanowire structure stability than the un-functionalized Zn_3P_2 nanowires against water-degradation, and better photocatalytic activity as well. The alkyne chain length in alkanedithiol functional groups affects photocatalytic activity of the functionalized Zn_3P_2 nanowires, for studied alkanedithiol functional groups with 1,3-PDT, 1,4-BDT and 1,12-DDT, as the alkyl chain decrease, the photocatalytic activity increases. The metal-doped Ag/Zn_3P_2 nanowires nanocomposite exhibits higher photocatalytic activity than the functionalized Zn_3P_2 nanowires, because the Fermi energy level of noble metal co-catalyst is lower than that of semiconductor; therefore facilitate charge transfer and mitigated photo-generated electron-hole recombination.

ACKNOWLEDGEMENTS

I would like to thank my committee chair, Dr. Zhengdong Cheng, and I would also like to thank my committee members, Dr.Ying Li and Dr. Perla Beatriz Balbuena, for their patience and valuable comments on my research works.

I would also like to thank my lab mates and my friends at Texas A&M University for their supports and inspirations.

Finally, I would like to thank my parents and my girlfriend for their encouragement and love.

NOMENCLATURE

eV	Electron-volts
Ag/Zn_3P_2	Silver and zinc phosphate nanocomposites
PES	Photoelectrochemical Synthesis Cells
OER	Oxygen Evolution Reaction
HER	Hydrogen Evolution Reaction
E_{cb}	Absolute energy for water splitting at surface under illumination for conduction band
E_{vb}	Absolute energy for water splitting at surface under illumination for valance band
-qE°	Electrochemical potentials
E°	Potential of reduction for (H^+/H_2) and (O_2/H_2O) redox couples
ΔG	Gibbs free energy change
SEM	Scanning Electron Microscopy
EDX	Energy-Dispersive X-ray spectroscopy
CVD	Chemical Vapor Deposition
UV	Ultraviolet
1,3-PDT	1,3-propanedithiol
1,4-BDT	1,4-butanedithiol
1,12-DDT	1,12-dodecanedithiol

UF	Un-functionalized Zn_3P_2 nanowires
k_{ET}	Rate of electron
k_0	Pre-exponential factor
β	Structure-dependent attenuation factor
$d_{D,A}$	Distance separating the donor and acceptor
I_0	Pre-exponential factor

TABLE OF CONTENTS

Page

LIST OF FIGURES

Page

LIST OF TABLES

Page

CHAPTER I

INTRODUCTION AND LITERATURE REVIEW

1.1 INTRODUCTION

Hydrogen energy is considered as the fuel of the future due to its abundance and no greenhouse emissions. Photochemical water-splitting process is considered as a zero-emission process. However, certain issues come up with photochemical water-splitting process such as inefficient use of solar spectrum, inefficient to consume the photo-generated electrons and holes in catalysis; and inefficient use of dissociated electrons and holes in catalysis. This thesis introduces the functionalized Zn_3P_2 nanowires that possess suitable optical properties and band diagram (~1.5eV[1], compare to 1.39 eV that is the ideal bandgap for efficient photovoltaics fabrication[2, 3]) for hydrogen production. Also, a vapor phase method, which yields uniform diameter of the functionalized Zn_3P_2 nanowires, will also be introduced to prevent low stability of the functionalized Zn_3P_2 nanowires and degradation of Zn in water-based solutions, therefore enhance the stability of the functionalized Zn_3P_2 nanowires nanostructure under photochemical reactions.

By functionalizing the Zn_3P_2 nanowires using alkanedithiol groups with different alkyl chain length, the relations between molecular structure and the rate of electron transfer will be studied, in order to choose suitable functional groups that can maximizes the photo-catalytic activity of the functionalized Zn_3P_2 nanowires in hydrogen

production. During the process of water splitting, which leads to the creation of free electrons and holes within the nanowires, fast electron-hole recombination process occurs. Therefore, strong reduction solvent such as methanol serves as a hole scavenger to avoid electron-hole recombination process and therefore the excited electrons are able to undergo the desired chemical reactions.

Based on previous review, it can be noticed that the main issue of the Zn_3P_2 nanowires is the degradation under photochemical reaction with water present in the solutions. Therefore using alkanedithiol functional groups to surface modify the Zn_3P_2 nanowires, in order to prevent nanowire structure integrity lose as well as increase photochemical reaction activity becomes the suitable approach to synthesize the functionalized Zn_3P_2 nanowires. Besides by studying the relationship between the structure integrity as well as photochemical reaction activity and different functionalized groups, later one can choose suitable alkanedithiol functional groups to functionalize Zn_3P_2 nanowires, and compare photochemical performance to select certain type of alkanedithiol functional group with highest photochemical activity, and using this selected the functionalized Zn_3P_2 nanowires to carry out photochemical.

By surface modify the Zn_3P_2 nanowires using organic functional groups; it can mitigate the limitation of application of the un-functionalized Zn_3P_2 nanowires as photocatalysis. Moreover, this method can improve charge transfer between the bulk materials and its surface, results faster charge separation and less electron-hole recombination. Photocatalysis that possesses the property that decelerate electron-hole recombination are more likely to generate free electrons and holes, which leads to faster

redox reaction in photochemical process, will lead to more hydrogen production. The thesis is the following these points:

The first results discussion in this thesis is: The photochemical hydrogen evolution comparison between un-functionalized Zn_3P_2 nanowires and functionalized Zn_3P_2 nanowires and their nanowire structure stability under water-based solutions. The un-functionalized Zn_3P_2 nanowires owns the low structure stability in water-based solution during photochemical reactions due to the chemical reaction of Zn_3P_2 with water to form zinc hydroxide. This chemical reaction gives the degradation in structure of the nanowires of Zn_3P_2 nanowires; therefore lost its structure integrity to preform photocatalytic reactions, causing the rate of hydrogen production decreases dramatically.

By surface modify the Zn_3P_2 nanowires with organic molecules, zinc atoms connected with organic functional groups that mitigate zinc phosphate reacting with water. Meanwhile the functional groups had been chosen have better performance in charge transfer between organic molecules and the Zn_3P_2 nanowires bulk surface, which in addition facilitate the charge transfer within the functionalized Zn_3P_2 nanowires, that possesses higher hydrogen production rate than the un-functionalized Zn_3P_2 nanowires. The alkanedithiol functional groups were chosen due to the trend to form zinc and sulfur chemical bond and its electron transfer preference. Because of the zinc atoms that bonding with organic molecules whom possess space volume on the surface of Zn_3P_2 nanowires, it could further prevent the diffusion of water onto zinc atoms surface to form zinc hydroxide, therefore improve the structure stability of Zn_3P_2 nanowires.

The second results discussion in this thesis is: The investigation of dependence of the functionalized Zn_3P_2 nanowires photochemical reaction activity on alkyl chain length of alkanedithiol functional groups.

Increasing the functionalized Zn_3P_2 nanowires structure stability and reaction activity in photochemical reactions. Synthesized the functionalized Zn_3P_2 nanowires and modified by select organic functional groups to obtain surface modified Zn_3P_2 nanowires with high structure stability. Because the Zn atom that bonding with functional groups further prevent the diffusion of water onto Zn atom to form Zn hydroxide, therefore enhance the structure stability of the functionalized Zn_3P_2 nanowires. This could be also explained due to the different surface coverage of the functionalized Zn_3P_2 nanowires. Functional groups with shorter alkyl chain length occupy less volume size in space; hence possesses larger percentage of surface coverage of the functionalized Zn_3P_2 nanowires.

The dependence of the functionalized Zn_3P_2 nanowires photochemical reaction activity on alkyl chain length of alkanedithiol functional groups was investigated. The electron transfer rate between hydrogen production rate and alkanedithiol groups with different alkyl chain length was also investigated. The electron can transport from the functionalized Zn_3P_2 nanowires bulk surface to the organic molecule by tunneling, and the rate of electron transfer also has influence on the electron transfer. Therefore the total reaction rate is limited by the tunneling rate and rate of electron transfer in the case of long alkyl chain. This investigation can also serves the application of select suitable organic functional groups to surface modify Zn_3P_2 nanowires.

The third results discussion in this thesis is: The hydrogen production rate comparison between the functionalized Zn_3P_2 nanowires and synthesized Ag/Zn_3P_2 nanocomposite photocatalysis.

The silver metal particles have influence on the electron transfer rate of the functionalized Zn_3P_2 nanowires bulk surface, the photo-generated electrons from the conduction band of the functionalized Zn_3P_2 nanowires transfer to the surface of silver particles, which change the electronic confinement on the functionalized Zn_3P_2 nanowires surface due to the Fermi level of metal always lower than the Fermi level of semiconductor. Therefore introduce the metal in the functionalized Zn_3P_2 nanowires mitigated the photo-generated hole and electron recombination process, and perform higher photochemical reaction activity compare to the functionalized Zn_3P_2 nanowires itself. The synthesized Ag/Zn_3P_2 nanocomposite photocatalysis can be considered as facilitate electron transfer from the functionalized Zn_3P_2 nanowires bulk surface to silver surface during the photochemical reactions. Moreover, the photo-generated electrons can be transfer by tunneling effect from the functionalized Zn_3P_2 nanowires bulk surface to functionalized alkyl chain groups, however abundant photo-generated electrons were still kept on the functionalized Zn_3P_2 nanowires bulk surface, the silver particles coated on the functionalized Zn_3P_2 nanowires bulk surface can serve as the reduction sites that react with hydrogen protons to generate hydrogen gases, thus increase the hydrogen production rate of Ag/Zn_3P_2 nanocomposite photocatalysis.

1.2 LITERATURE REVIEW

Solar energy occupies tremendous energy source with 3.0×10^{24}J a year, and world energy consumption is 5.0×10^{20}J a year[4]. With only 10% efficiency conversion of 0.1% solar energy would meet the demand of current energy need[5]. However the world's energy are majorly provided by consumption of fossil fuels. Figure 1 shows the world's fuel shares according to different types of energy sources, shares of electricity generated by energy categories, and carbon dioxide emissions in year 2011. The combination energy comes from the oil, coal/petroleum and natural gas are 82% that dominated the energy resources.

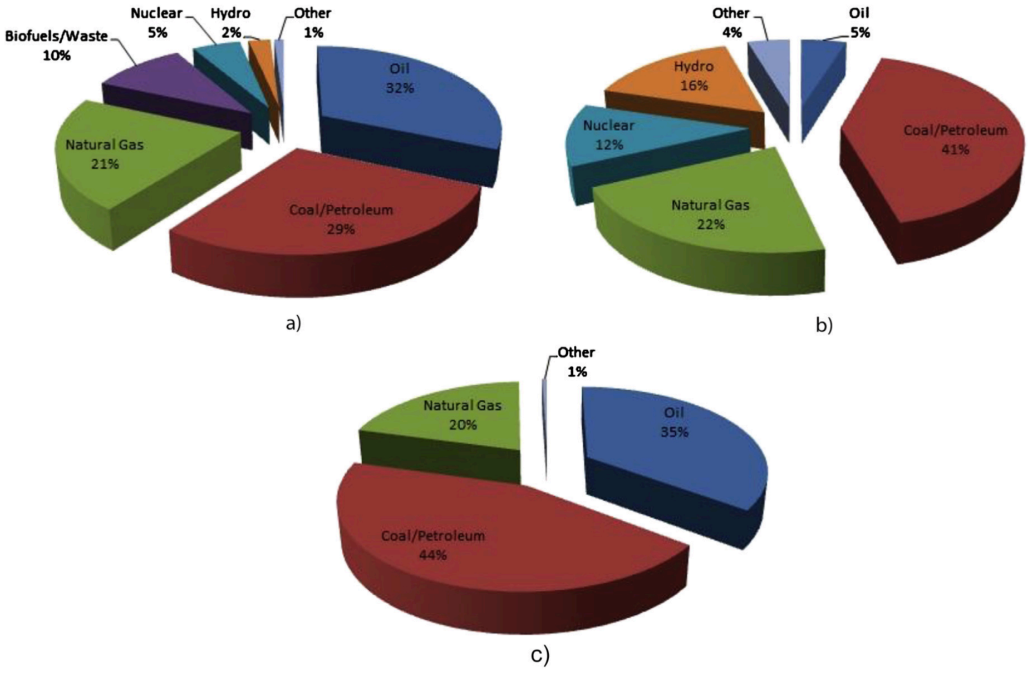

Fig. 1 World wide energy portions of (a) percentage of different types of energy, (b) electricity generated by energy categories, and (c) carbon dioxide emissions by energy categories in the year of 2011[6].

Among those different types of solar energy, hydrogen energy only consists of 2% among those energy categories. The 85% of global energy are generated by fossil fuel, while due to its limited resources and unbalanced distribution, fossil fuel are not expected to meet the growing energy demand of energy consumption boom. Also the fossil fuels under oxidation reaction are generating greenhouse gas (carbon dioxide) that also generates environmental issues in recent years.

On the one hand, the key issues of converting fossil fuels into energy are greenhouse gases emission and sulfur contained gases emission, such as CO_2, SO_2 that facilitate the process of global warming and environmental pollution[7]. If the energy share continues maintain fossil fuel dominated structure, human beings will encounter serious environment consequences. Therefore, in order to achieve sustainable human society development, the development of the clean and renewable energy resources are imminent[7]. And the solar energy is considered as no greenhouse gases emission process of energy transformation. According to the Intergovernmental Panel on Climate Change Synthesis Report 2007, there is a clear link between greenhouse emissions and global warming[8]. And by selecting the altered clean energy resources other than fossil fuels are urgent for human civilization development.

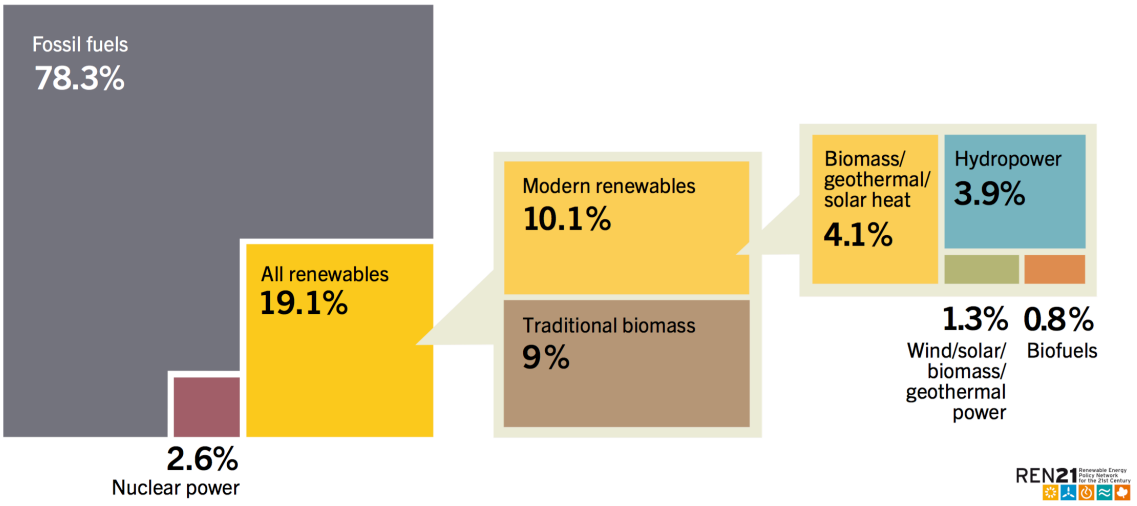

Fig. 2 Renewable energy resources share by categories of world energy total consumption estimation in the year of 2013[9].

Figure 2 shows the renewable energy resources share by categories of world energy total consumption estimation in the year of 2013. However the combination of the solar and other renewable energy sources only contribute less than 2% of the total electricity production[9]. And the global energy need has been rising by 1.5% annual in recent years[10]. Despite the fact that world energy consumption increasing continuously, the greenhouse gas emissions remain stable in the year 2014[11]. The stable carbon dioxide emission stability in the year 2014 was owned to the increase consumption of renewable energy and optimization of effectively conversion of energy. The trend of energy share transformation is undergoing a mild process in the world global energy consumption.

On the other hand, the water splitting photochemical reaction generated hydrogen energy is considered as the “future energy” due to its high conversion efficiency, high

energy capacities in energy storage, with HHV 141.9 (kJ/g)[12] and zero pollution process. However, currently only 5% of the hydrogen production came form photochemical water-splitting process[13], the majority of commercial used hydrogen are converted from the fossil fuel, therefore huge proportion of hydrogen energy transformation share can be developed by using water-splitting process. Photochemical water-splitting process will become more favorable[14] in the near future for converting hydrogen energy due to the improvement of efficiency and photochemical catalysis cost reduce. The advantages of using hydrogen energy as the major energy sources are[15]: (i) energy conversion efficiencies is high, meaning less energies are used to generated hydrogen; (ii) zero greenhouse gas emissions in hydrogen production process, due to the absorption of energy comes from photonic energy (solar irradiation); (iii) production raw resources abundance, water resources are abundant on earth; (iv) high energy-density storage and transportation convenience etc.

Hydrogen can be produced by photosynthesis reactions such as using the photoelectrochemistry method to obtain photoelectrochemical synthesis (PES) cells in organic waste water treatment to generate electricity and hydrogen, these research works have been heavily studied by [16-21], multifunctional assemblies and membrane assemblies in natural photosynthesis[22], and semiconductor based photocatalytic reactions.

The semiconductor based photocatalysis development traced back into 1980s when research works focused on $SrTiO_3$ and TiO_2 semiconductors[23, 24]. To date quiet amount of photocatalysis have been studied for water splitting such as highly active

photocatalyst ZrO_2[25] without co-catalysis, TiO_2 combined with SnO_2, ZrO_2, Cu_xO, and Ag_xO as co-catalysis[26] and TiO_2 doping with Pt, Ga and RuO_2[27-31], titanates photocatalysis such as $Na_2Ti_3O_7$, $K_2Ti_2O_5$, and $K_2Ti_4O_9$[32], NiO/Ni co-catalysis[33], $PbWO_4$-RuO_2 co-catalysis[34], GaN doped with Zn^{2+} [35-37].

As for photochemical catalytic reactions, the photocatalysis converts photonic energy (comes from solar irradiation) to chemical energy (hydrogen)[13, 38]. The energy carried by the photon is proportional to the frequency of the radiation and given by hν where h stands for the Planck constant and ν stands for the frequency of the photon[39]. When a photon hits the photochemicalcatalyst, a photochemical reaction develops a photo-generated electron and photo-generated hole, which comes in pair in the photochemicalcatalyst, the obtained photo-generated electrical charge is used to undergo reduction the hydrogen proton in the reaction aqueous to hydrogen. In order for a photochemicalcatalyst to split water and generate hydrogen, it should have an appropriate band gap and properly located conduction and valance bands for oxidation/reduction reactions[15].

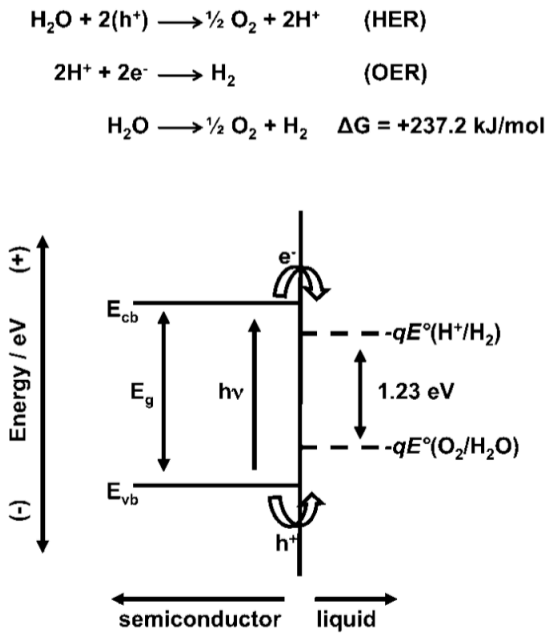

Fig. 3 Oxidation reaction and reduction reaction for overall water splitting process; and band gap position of the ideal semiconductor compare to electrical photochemical potential of overall water splitting process[40].

The water-splitting energy is calculated as 1.23eV, derived from the change of Gibbs free energy of synthesis one molecule water from hydrogen and oxygen (ΔG = 237.2 kJ/mol) as shown in figure 3. Ideally the energy requires for splitting the water is 1.23eV, however in order to drive the reaction, and considered the thermodynamic laws as well as chemical kinetics considerations, the over-potential effective photo-voltage needs to be at least 2.4eV to ensure overcome the photochemical reaction potential[41].

Among the photocatalysts that been used for water splitting, several requirements of material properties have to met certain requirements, suitable photochemical catalysts for hydrogen production have to meet certain criteria[42]: 1.Visible light absorption (mostly 390nm-700nm). 2. High chemical stability for water splitting. 3. Suitable band

gap positions to enable reduction/oxidation of water as mentioned before. 4. Fast electron transfer rate in the bulk and surface of semiconductor to mitigate the hole-electron recombination. 5. Low over potential for the reduction/oxidation reaction, and 6. Low cost of photocatalysts materials or synthesis process[43]. Metallic oxides photocatalysts that possess large band gap (SnO_2,TiO_2)[44] cannot use solar energy efficiently. Although sulfides oxides photocatalysts have narrow band gap (higher absorption of solar energy), but sulfides oxides photocatalysts (such as CdS)[45] are less stable and easily have undergo the photochemical and chemical reactions with photochemical reaction solutions.

However, the functionalized Zn_3P_2 nanowires structure possess suitable optical properties and band diagram for hydrogen production, besides the earth abundant materials Zn_3P_2 can lower the cost of photochemical catalysts, it has been tested the least expensive among 23 compounds[46]. However the major issue with the Zn_3P_2 nanowires is its low structure stability in water-based solution during photochemical reactions, which will cause degradation of the Zn_3P_2 nanowires in water based photochemical reaction solution[47]. While a chemical vapor deposition method[48] were carried out to assist synthesis the functionalized Zn_3P_2 nanowires by using alkanedithiol as well as organic functional groups, in order to prevent nanowire structure degradation as well as increase photochemical reaction activity, which can yield higher hydrogen production amount and maintain reaction activity in long period of time. Moreover, this chemical vapor deposition method offers several advantages, such as resistance against degradation caused by moisture and air, to the functionalized Zn_3P_2 nanowires. The

functionalized Zn_3P_2 nanowires modified by the alkanedithiol groups can increase the electron transfer rate from the bulk nanowires to its surface and improve the stability to against photo-degradation[49].

Furthermore, the noble metal (such as Au, Ag, Pd, Pt and Rd) served as co-catalysts have been studied heavily, Au particles doped on the TiO_2 (N-TiO_2)[50], and Au, Ag particles coated on the TiO_2 films[51-53] have been improved to increase the hydrogen production efficiency of the semiconductor photocatalysis. By irritating the silver particles on the functionalized Zn_3P_2 nanowires could facilitate the charge transfer from Zn_3P_2 nanowires bulk surface to the silver nanoparticles as well as mitigate the electron-hole recombination on the nanowire surface, which in turns facilitate the hydrogen production rate.

CHAPTER II

EXPERIMENT METHODS

2.1 INTRODUCTION

Zinc phosphide (Zn_3P_2) nanowires were synthesized using chemical vapor deposition (CVD) method by exposing zinc phosphide powder source in a hot-wall chamber. Functionalized Zn_3P_2 nanowires were accomplished by using in *situ* functionalization method exposing Zn_3P_2 nanowires to the organic functional groups vapor[48]. Ag nanoparticle deposited on Zn_3P_2 nanowires nanocomposite were synthesized by using ultraviolet (UV) light deposition method. Zn_3P_2 nanowires, functionalized Zn_3P_2 nanowires and Ag/Zn_3P_2 nanocomposite were characterized by energy-dispersive X-ray spectroscopy (EDX) and scanning electron microscopy (SEM), and those photocatalysis were evaluated by the photocatalytic hydrogen evolution setup.

2.2 Zn_3P_2 NANOWIRES SYNTHESIS AND ITS FUNCTIONALIZATION

Zn_3P_2 nanowires were synthesized using chemical vapor deposition method. The hot-wall chamber consists with two separated zones, precursor decomposition zone and deposition zone, both zones are heated under different temperature as shown in figure 4.

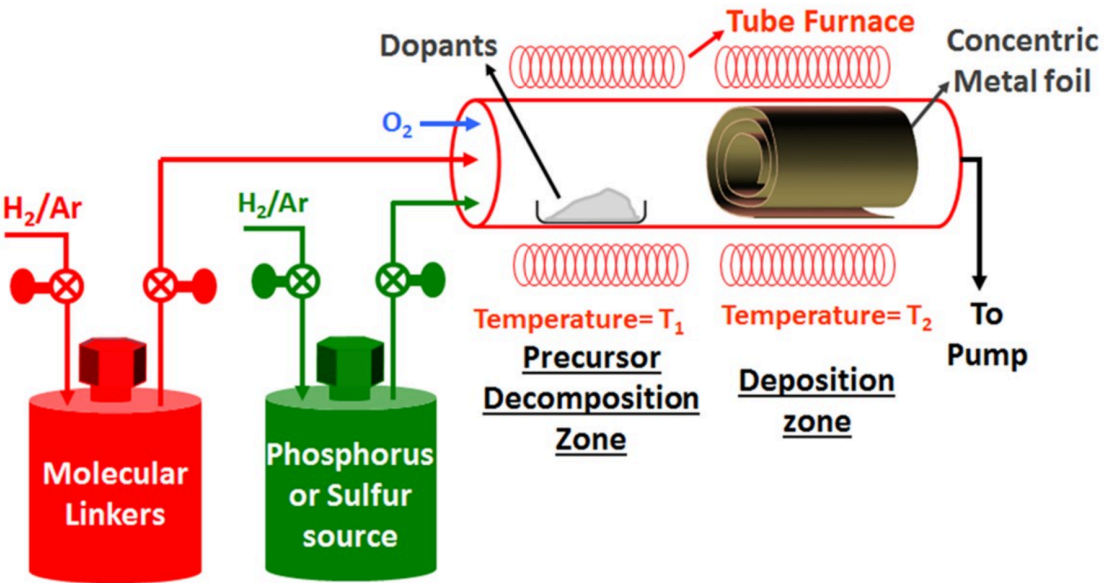

Fig. 4 Schematic of the three-zone tube furnace employed for the synthesis and in-situ functionalization[48].

We were using zinc phosphide powder as the source of precursor and zinc foil as the deposition substrate, operated in desired upstream and downstream temperature, pressure conditions and desired carrier gas conditions. The functionalized Zn_3P_2 nanowires were obtained by exposing the Zn_3P_2 nanowires to organic molecular vapor conditions right after the synthesis of Zn_3P_2 nanowires, the different functional organic molecular groups are exposing under their correlated vaporizing temperatures. The Zn_3P_2 nanowires functionalization was using 1,3-propanedithiol (1,3-PDT), 1,4-butanedithiol (1,4-BDT) and 1,12-dodecanedithio (1,12-DDT) as the organic molecular groups for the study.

2.3 Ag/Zn_3P_2 NANOCOMPOSITE SYNTHESIS

Ag nanoparticles were deposited on the functionalized Zn_3P_2 nanowires in order to synthesis the Ag/Zn_3P_2 nanocomposite. The detailed experiments method are described as follow: the obtained functionalized Zn_3P_2 nanowires substrate was weighted using AR3130 (OHAUS Corp. Pine Brock, NJ) scale to measure the weight (w_1) of the substrate, the weight combination of the zinc substrate and the functionalized Zn_3P_2 nanowires. After that the functionalized Zn_3P_2 nanowires foil was put into a 250 mL Pyrex water-jacketed round bottom flask with 5mL Milli-Q water, then placed the 250 mL Pyrex water-jacketed round bottom flask was under ultra-sonication (50W, UD50SH-1.8LQ, RoHS) in 20°C for 20 minutes to remove the nanowires on the zinc substrate in order to obtain the functionalized Zn_3P_2 nanowires water solution. Then remove the zinc substrate from the water-jacketed round bottom flask, washed with 5mL Milli-Q water, then put after-washed solution into the flask, obtained the functionalized nanowires solutions (w_1-w_2) gram functionalized nanowires in 10 mL Milli-Q water. And dried the zinc substrate in drying oven under 60°C overnight, then measure the weight of dried zinc substrate (w_2). The weight difference $\Delta w=w_1-w_2$ is the weight of the obtained functionalized Zn_3P_2 nanowires. The obtained functionalized Zn_3P_2 nanowires water solution was added desired amount (1wt% of Δw) of silver nitrate solution (Fisher, 1M) for reduction of sliver on the functionalized Zn_3P_2 nanowires.

The photo-deposition of silver nanoparticles on the functionalized Zn_3P_2 nanowires method was accomplished by UV light deposition. First put the water-jacketed round bottom flask in ultra-sonication (50W, UD50SH-1.8LQ, RoHS) under

20°C for 10 minutes in order to well dispersed the functionalized Zn_3P_2 nanowires and the silver nitrate solutions, at the meantime put the magnetic stirring bar in to the water-jacketed round bottom flask. And then placed the water-jacketed round bottom flask under a 100 watts standard long wave ultraviolet lamp (Model B-100AP MDSK, Upland, CA) as the source of ultraviolet (UV) light for 1 hour with magnetic stirring bar (60rpm, 25°C) to initiate the oxidation-reduction photochemical reaction to deposit silver nanoparticles on the 1,3-PDT functionalized Zn_3P_2 nanowires.

2.4 PHOTOCATALYTIC HYDROGEN EVOLUTION

2.4.1 Photocatalytic hydrogen evolution reaction for the functionalized Zn_3P_2 nanowires.

All the functionalized Zn_3P_2 nanowires with three different organic functional groups photocatalytic hydrogen evolution reaction was carried out in a 250 mL Pyrex water-jacketed round bottom flask. First of all, seal-leakage test on the 250 mL Pyrex water-jacketed round bottom flask was performed before any experiments to ensure no hydrogen gas leakage during photocatalytic hydrogen evolution reaction process. The silicon septum was sealed tightly on the empty flask, and then connected to a nitrogen gas input source (200psi) with syringe needle insert through the silicon septum for 2 minutes. The pressurized 250 mL Pyrex water-jacketed round bottom flask was put into water to detect possible bubbles around the silicon septum. If there was no bubble around the silicon septum, then performed the photocatalytic hydrogen evolution, if there was bubble, replace the silicon septum and repeat the seal-leakage test.

All experiments of photocatalytic hydrogen evolution performed are contains the total amount volume of solution 150 mL, contains both methanol (Certified ACS, 99.8%, Fisher Chemical) aqueous solution and Milli-Q water. In the experiment of test photocatalytic hydrogen evolution of Ag/Zn_3P_2 nanocomposite, small amount of silver nitrate (1wt% of Δw) was introduced to the photocatalytic hydrogen evolution system, due to its limited amount (~uL) compare to reaction solution volume (150mL), therefore the remaining silver nitrate in the system was considered as negligible amount in volume percentage. Figure 5 shows the schematic photocatalytic hydrogen evolution reaction for the functionalized Zn_3P_2 nanowires.

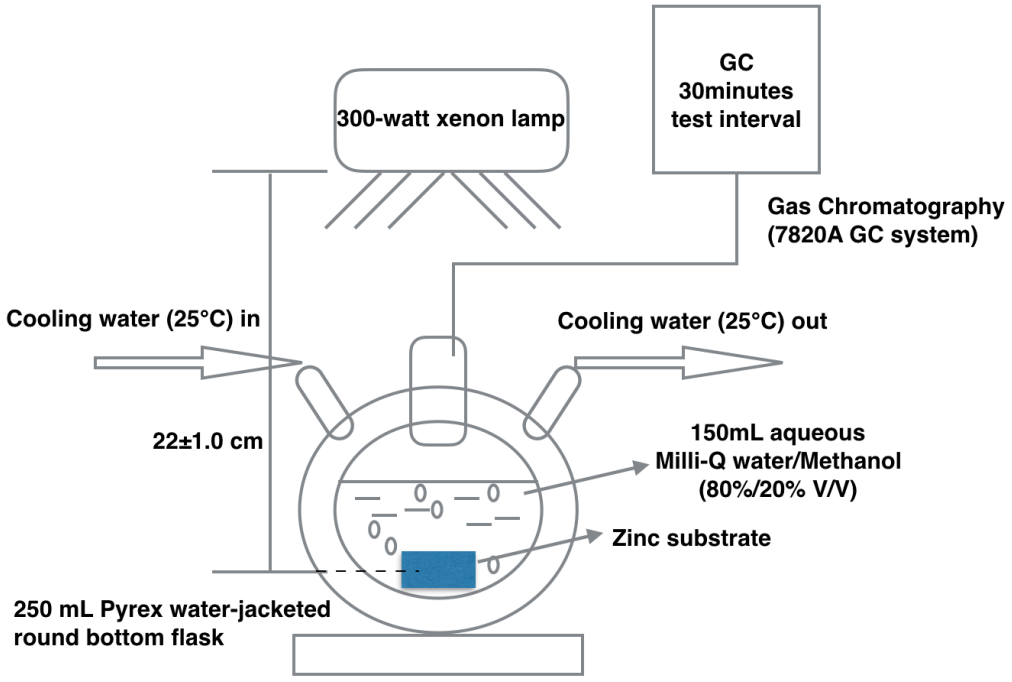

Fig. 5 Schematic photocatalytic hydrogen evolution reaction for the functionalized Zn_3P_2 nanowires.

In the photocatalytic hydrogen evolution test of the three different functionalized Zn_3P_2 nanowires with 1,3-propanedithiol (1,3-PDT), 1,4-butanedithiol (1,4-BDT) and 1,12-dodecanedithio (1,12-DDT), the volume ratio of methanol and Milli-Q water was controlled as (20%/80% V/V), 30mL methanol aqueous solution with 120mL Milli-Q water.

First the 150mL hydrogen evolution solution was mixed vigorously by a magnetic stirring bar (100rpm) in water-jacketed round bottom flask for 10 minutes under ambience temperature. Second the methanol/water solution was under ultra-sonication (50W, UD50SH-1.8LQ, RoHS) in 20°C for 20 minutes to remove any gases solved in the methanol and Milli-Q water. Third the zinc substrate coved with functionalized Zn_3P_2 nanowires was measured weight before (w_b) photochemical hydrogen evolution that could calculate the weight of functionalized nanowires to normalize the rate of hydrogen production.

The functionalized Zn_3P_2 nanowires with zinc substrate were introduced into the 150mL methanol and Milli-Q water aqueous solution, and after that the water-jacketed round bottom flask was degassed for 30 minutes using nitrogen gas to remove the oxygen in the water-jacketed round bottom flask, in order to prevent photo-generated hydrogen react with oxygen in the water-jacketed round bottom flask. The photocatalytic hydrogen evolution was carried out under a 300-watt xenon lamp (PE300BF, Cermax) as the visible light source. Figure 6 shows the spectral output wavelength for the 300-watt xenon lamp. By applying F + HOT MIRROR, the light spectrum mainly laid on 380nm-780nm.

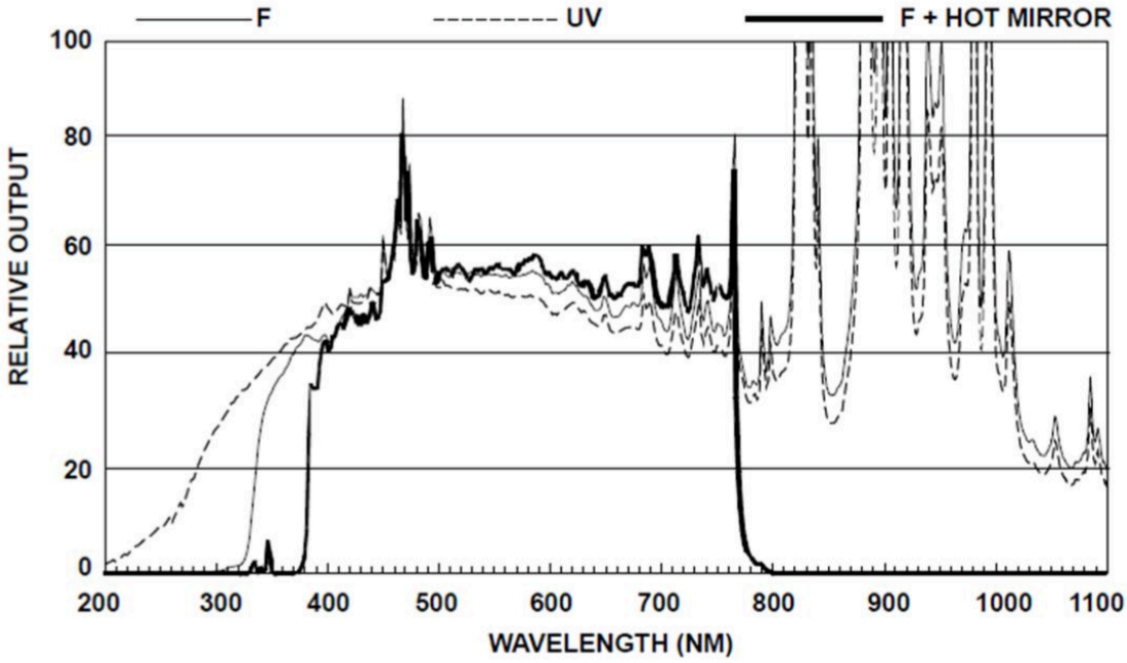

Fig. 6 Spectral output wavelength for PE300BF CERMAX® XENON ARC LAMPS.

The functionalized Zn_3P_2 nanowires substrate in the 250 mL Pyrex water-jacketed round bottom flask laid on the focus distance of xenon lamp, and visible light covers entire area of zinc substrate, to ensure maximum visible light intensity of full area. The distance between the 300-watt xenon lamp visible light source and the photocatalysis was 22±1.0 cm; horizontal and vertical light intensity were measured by using a light intensity meter (PLMT68, PYLE) and the maximum light intensity was observed on the photocatalysis was 36.8±3.3 mW/cm^2.

Circulating cooling water was used in 250 mL Pyrex water-jacketed round bottom flask with water recirculating cooling system to maintained the photocatalytic hydrogen evolution reaction at 25°C for all photocatalytic hydrogen evolution experiments.

The amount of produced hydrogen was extracted from Pyrex water-jacketed round bottom flask by a 500uL syringe, and extracted hydrogen was analyzed every 30 minutes for 4 hours using gas chromatography (Agilent Technologies, 7820A GC system) with a 5-Å molecular sieve column used for the thermal conductivity detector. The split-splitless was set on the split mode with split ratio 9:1 (18mL/min), the inlet at the back of gas chromatography, the heater was set at 120°C and the pressure was set at 1.1338 psi. The gas saver was set on with 20mL/min and 6 min afterwards.

After the photocatalytic hydrogen evolution, the 250 mL Pyrex water-jacketed round bottom flask was undergone ultra-sonication (50W, UD50SH-1.8LQ, RoHS) in 20°C for 20 minutes to remove the functionalized Zn_3P_2 nanowires on the zinc substrate. The afterwards solution was kept to characterize morphology of functionalized Zn_3P_2 nanowires after photocatalytic hydrogen evolution.

The zinc substrate was washed thoroughly using deionized water and dried in oven under 60°C overnight, then measure the weight of dried zinc substrate after (w_a) the photocatalytic hydrogen evolution. The weight difference $\Delta w=w_b-w_a$ is the weight of the functionalized Zn_3P_2 nanowires involved in photocatalytic hydrogen evolution. In the normalize calculation of photocatalytic hydrogen evolution rate, the weight difference of

the functionalized Zn_3P_2 nanowires was divided by amount of hydrogen generated per hour, which gave the hydrogen production rate with unit umol/g/h.

2.4.2 Photocatalytic hydrogen evolution reaction for Ag/Zn_3P_2 nanocomposite.

Prior to the photocatalytic hydrogen evolution reaction, synthesized the Ag/Zn_3P_2 nanocomposite that mentioned above was obtained in 10mL Milli-Q water solution with negligible amount of nitrate ions. This nanocomposite solution was considered as the photocatalysis, the same as previous the functionalized Zn_3P_2 nanowires solutions with Milli-Q water and methanol, operated in similar conditions.

The following photocatalytic hydrogen evolution procedures are as the same as the photocatalytic hydrogen evolution reaction for the functionalized Zn_3P_2 nanowires. Figure 7 shows the schematic photocatalytic hydrogen evolution reaction for Ag/Zn_3P_2 nanocomposite. However the 10mL solvent Milli-Q water, which dissolve the Ag/Zn_3P_2 nanocomposite, had to be deducted by the total amount of Milli-Q water added later in to the system. In other words, another 110mL Milli-Q water were added in to the photocatalytic hydrogen evolution system with 30mL methanol aqueous solutions to keep total amount volume of reaction solution as 150mL.

After obtained 150mL reaction solution that contains Ag/Zn_3P_2 nanocomposite, Milli-Q water, methanol aqueous solution and negligible nitrate ions, the photocatalytic hydrogen evolution was carried out with a magnetic stirring bar in the system without stirring during the entire photocatalytic hydrogen evolution reaction, this magnetic

stirring bar served as the similar function of zinc substrate, which to provide attachment surface of Ag/Zn_3P_2 nanocomposite.

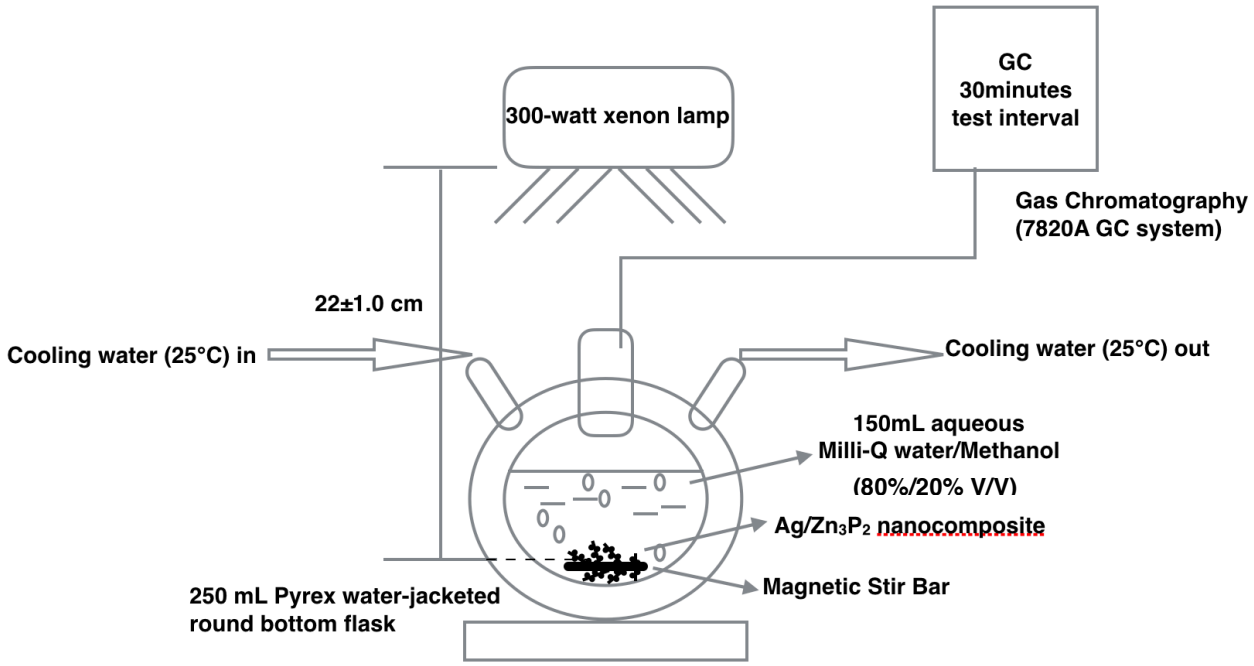

Fig. 7 Schematic of photocatalytic hydrogen evolution reaction for Ag/Zn_3P_2 nanocomposite.

The Ag/Zn_3P_2 nanocomposites were collected on the surface of magnetic stirring bar or at the bottom of the 250 mL Pyrex water-jacketed round bottom flask due to gravitational force, similar to previous exposing area, the magnetic stirring bar laid on the focus distance of xenon lamp, and visible light covers entire area where collected Ag/Zn_3P_2 nanocomposite, to ensure the same maximum visible light intensity of full area compare to which exposed to zinc substrate.

2.5 CHARACTERIZATION OF PHOTOCATALYSTS

Characterization of morphology method was introduced before and after the photocatalytic hydrogen evolution of both functionalized Zn_3P_2 nanowires and Ag/Zn_3P_2 nanocomposite respectively. The Quanta 600 FEG field emission scanning electron microscope (SEM) from Microscopy and Imaging Center was used to observe the functionalized Zn_3P_2 nanowire and the Ag/Zn_3P_2 nanocomposite structure. And the Oxford EDS characterization system equipped with X-ray mapping and digital imaging associated with the Quanta 600 was used to characterize the elemental analysis of the Ag/Zn_3P_2 nanocomposite.

ImageJ software was used to accompany with SEM images to measure the size of the functionalized Zn_3P_2 nanowire and the Ag/Zn_3P_2 nanocomposite. The principle of ImageJ software image processing is to use statistical calculation of the pixel values of the scale bar on the SEM images and compare to the pixel values of the diameter of the functionalized Zn_3P_2 nanowire and the diameter of Ag particles of Ag/Zn_3P_2 nanocomposite in that images. By applying this method the nano-meter scale size of the functionalized Zn_3P_2 nanowire and the Ag/Zn_3P_2 nanocomposite can be measured accurately with micron-meter scale bar. Table 1 and table 2 shows the diameter measurement of the Zn_3P_2 nanowires and the Ag particles on the Ag/Zn_3P_2 nanocomposite. The diameter of the functionalized Zn_3P_2 nanowires is 55.71±9.54 nm and the diameter of Ag particles on the Ag/Zn_3P_2 nanocomposite is 66.03±12.33 nm.

Table 1. Diameter of the functionalized Zn_3P_2 nanowires measurement.

Number	Area	Mean	Angle	Length	Actual value (nm)
1	0.008	63.67	0	0.225	65.50
2	0.006	51.127	45	0.173	50.36
3	0.005	56.865	-45	0.16	46.58
4	0.007	62.747	26.565	0.207	60.27
5	0.005	58.267	45	0.133	38.72
6	0.006	40.889	51.34	0.188	54.74
7	0.005	37.702	-36.87	0.15	43.67
8	0.006	43.646	-30.964	0.177	51.53
9	0.008	49.074	23.199	0.224	65.22
10	0.005	49.452	53.13	0.153	44.55
11	0.007	68.45	-26.565	0.207	60.27
12	0.006	57.053	-30.964	0.177	51.53
13	0.008	63.377	0	0.225	65.51
14	0.007	61.238	18.435	0.193	56.19
15	0.008	71.407	-29.745	0.226	65.80
16	0.007	58.776	38.66	0.195	56.77
17	0.008	63.219	90	0.225	65.51
18	0.009	61.612	-35.538	0.256	74.53
19	0.006	63.032	0	0.167	48.62
20	0.005	51.7	21.801	0.158	46.00
21	0.005	43.17	21.801	0.149	43.38
22	0.008	52.065	45	0.25	72.79
23	0.007	45.847	33.69	0.21	61.14
24	0.007	54.075	45	0.216	62.89
25	0.006	45.016	45	0.173	50.37

Table 1. Continued

Number	Area	Mean	Angle	Length	Actual value (nm)
Mean					55.71
Standard deviation					9.54

Table 2. Diameter of Ag particles on the Ag/Zn_3P_2 nanocomposite measurement.

Number	Area	Mean	Angle	Length	Actual value (nm)
1	14	154.308	-32.471	13.408	83.63
2	10	135.2	0	9	56.13
3	10	176.991	32.005	9.339	58.25
4	12	190.149	-29.055	10.919	68.10
5	8	120.623	-90	6.667	41.58
6	14	163.107	0	12.5	77.96
7	10	168.706	-90	9.014	56.22
8	11	172.749	21.801	10.308	64.29
9	10	174.526	-35.538	9.014	56.22
10	12	140.375	0	11.333	70.68
11	12	148.139	0	11	68.61
12	12	170.843	48.814	10.853	67.69
13	13	140.288	-19.983	12.019	74.96
14	10	146.945	5.711	9.339	58.25
15	9	139.62	0	8.333	51.97
16	9	186.349	-90	7.667	47.82
17	13	130.062	-37.875	11.823	73.74
18	14	208.587	28.61	12.579	78.46

Table 2. Continued

Number	Area	Mean	Angle	Length	Actual value (nm)
19	11	187.091	-36.87	9.804	61.15
19	11	187.091	-36.87	9.804	61.15
20	14	147.079	4.399	13.004	81.11
21	12	162.269	-33.69	10.541	65.74
22	17	226.705	31.608	15.723	98.06
23	12	196.966	-37.875	11.47	71.54
24	12	207.114	-90	10.5	65.49
25	10	139.372	0	8.5	53.01
Mean					66.03
Standard deviation					12.33

The functionalized Zn_3P_2 nanowires with 1,3-propanedithiol (1,3-PDT), 1,4-butanedithiol (1,4-BDT) and 1,12-dodecanedithio (1,12-DDT) functional groups are characterized by SEM to observe structure morphology before any photocatalytic hydrogen evolution, thus provided evidence for comparison of structure integrity and nanowire degradation with characterization results after photocatalytic hydrogen evolution. The SEM characterization of the functionalized Zn_3P_2 nanowires before photocatalytic hydrogen evolution was preformed by cutting zinc substrate directly to make SEM samples and observed the morphology of functionalized Zn_3P_2 nanowires on the zinc substrate. The SEM images before functionalized Zn_3P_2 nanowires photocatalytic hydrogen evolution are known as the “solid based” images. The SEM characterization of the functionalized Zn_3P_2 nanowires after photocatalytic hydrogen

evolution was preformed by observed solutions that contained the functionalized Zn_3P_2 nanowires after the photocatalytic hydrogen evolution. The SEM images after functionalized Zn_3P_2 nanowires photocatalytic hydrogen evolution are known as the "liquid based" images.

CHAPTER III

RESULTS AND DISCUSSIONS*

3.1 FUNCTIONALIZED AND UN-FUNCTIONALIZED NANOWIRES

The key issue with the un-functionalized Zn_3P_2 nanowires is its low structure stability in water-based solution during photochemical reactions. Water based solutions will cause photo-catalytic degradation of the un-functionalized Zn_3P_2 nanowires reacting with water and forming zinc hydroxide therefore lost its structure integrity to preform photocatalytic reactions:

$$Zn_3P_2 + 6H_2O \rightarrow 3Zn(OH)_2 + 2PH_3$$

The approach for mitigate zinc phosphate reacting with water was to cover the chemical bond of zinc atoms on the un-functionalized Zn_3P_2 nanowires with organic functional groups. The alkanedithiol functional groups, with two sulfur atoms at the two sides of its structure, were chosen due to the trend to formation zinc and sulfur chemical bond. Those alkanedithiol molecules have two sulfur-hydrogen terminations, and once the alkanedithiol molecules are adsorbed by the un-functionalized Zn_3P_2 nanowires, the sulfur-hydrogen bond from those alkanedithiol molecules break and the sulfur atoms form a new chemical bond with the zinc atom on the surface of bulk nanowires. Because of the zinc atoms that bonding with functional groups further prevent the diffusion of water onto zinc atoms to form zinc hydroxide, therefore enhance the structure stability of

*Reprinted with permission from "Investigation of Electron Transport Through Alkanedithoil of Functionalized Zn_3P_2 Nanowires for Hydrogen Production" by Li, H. and Z. Cheng, 2016. Int J Nano Stud Technol, S1, p. 1-5, Copyright [2016] by Int J Nano Stud Technol.

Zn_3P_2 nanowires, and moreover a better surface coverage percent on the functionalized Zn_3P_2 nanowires would result better photocatalytic structure stability against degradation.

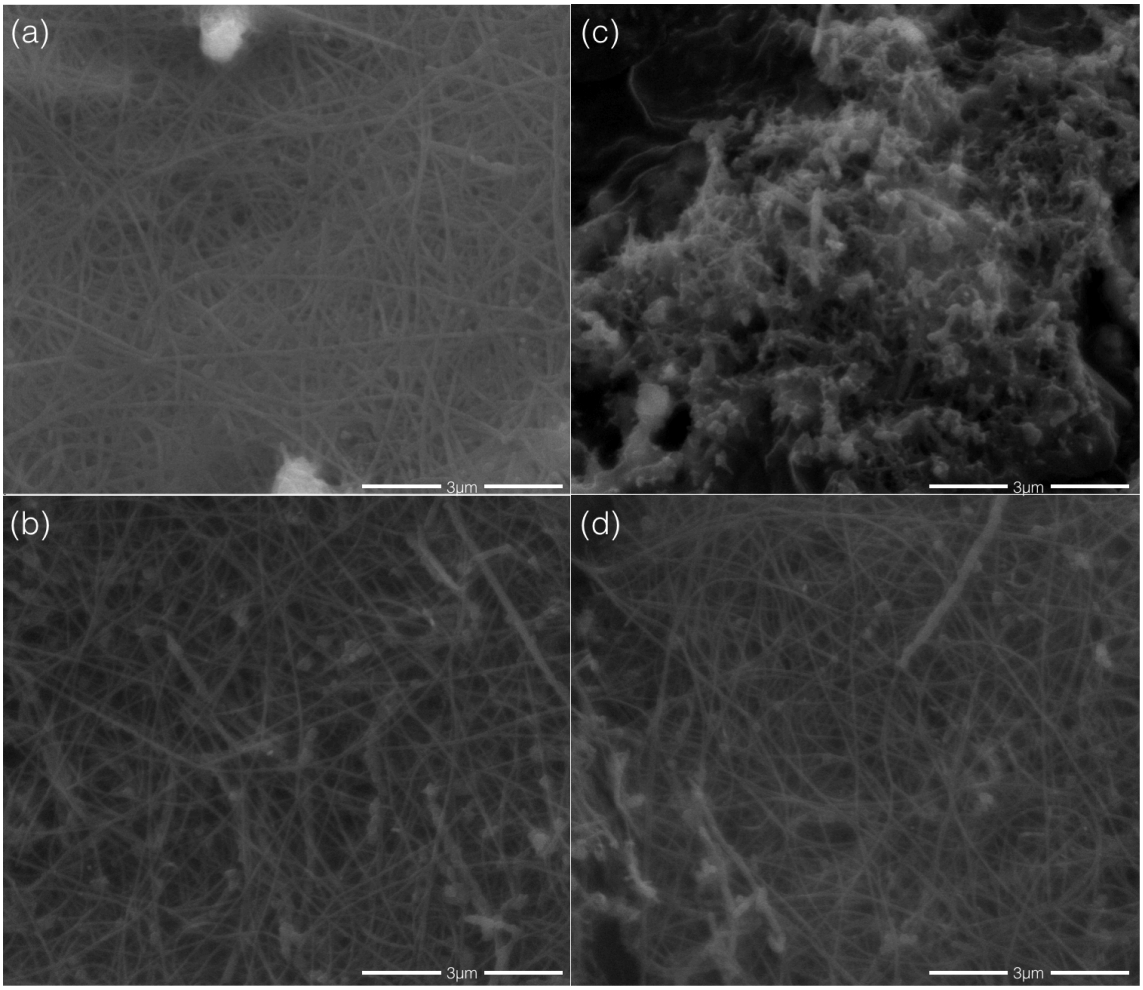

Fig. 8 SEM images of un-functionalized Zn_3P_2 nanowires and 1,4-BDT functionalized Zn_3P_2 nanowires respectively before (ab) and after (cd) suspend in deionized water for 10 day in room temperature.

Figure 8 shows the SEM images of the un-functionalized Zn_3P_2 nanowires and the 1,4-BDT functionalized Zn_3P_2 nanowires respectively before (ab) and after (cd) suspend in deionized water for 10 day in room temperature. As shown in Fig. 8a and b,

the Zn_3P_2 nanowires are kept in similar nanowire morphologies with diameter of the nanowires around 40-60 nm and length of the nanowires approximately ~10μm. Degradation caused by Zn_3P_2 nanowires react with deionized water occurs in the un-functionalized Zn_3P_2 nanowires. The nanowires structure degradation with water in morphologies transformed wire-structure into small particles combined with discontinuous shorter nanowires and degraded into discontinuity surface compare to the web-like nanowire structures. However the 1,4-BDT functionalized Zn_3P_2 nanowires maintain its nanowire morphology after suspended in deionized water for 10 day, the ability to against water caused degradation is because of the surface reconstruction during functionalization of the Zn_3P_2 nanowires as well as higher surface coverage that enhancing the structure stability against the degradation. As for photochemical activity of hydrogen production regarding to the un-functionalized Zn_3P_2 nanowires and the 1,4-BDT functionalized Zn_3P_2 nanowires. Prediction of the photochemical activity of photocatalysis can be made based on their structure stability. Without web-like nanowire structures and combine with Zn_3P_2 reacting with water and forming zinc hydroxide, the photochemical activity of the un-functionalized Zn_3P_2 nanowires will drop drastically during the photocatalytic hydrogen evolution reaction.

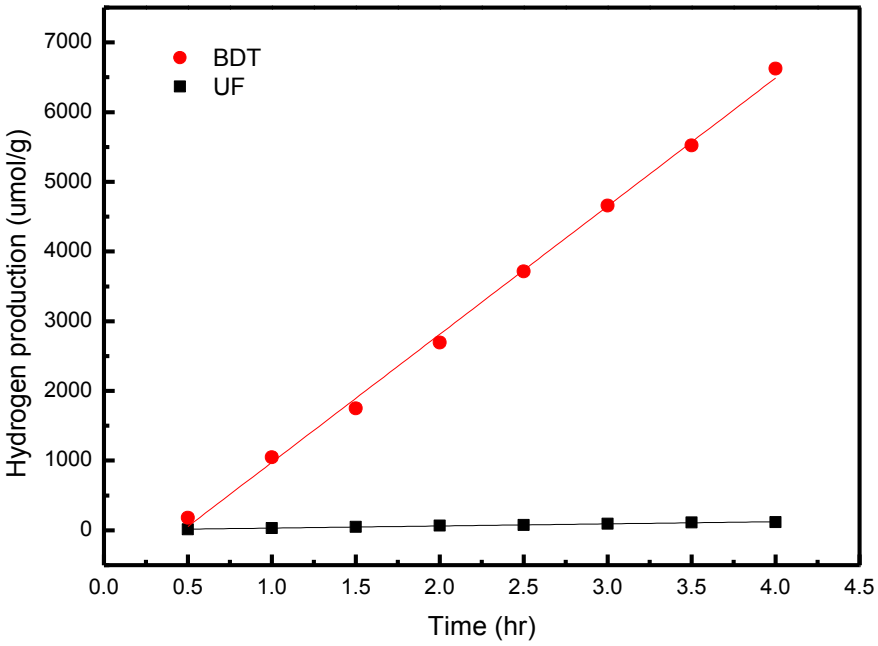

Fig. 9 Photocatalytic hydrogen evolution reaction results of the un-functionalized Zn_3P_2 nanowires (UF) and the 1,4-BDT functionalized Zn_3P_2 nanowires (1,4-BDT).

Figure 9 and table 3 shows the experiment results of amount of hydrogen production performance of the un-functionalized Zn_3P_2 nanowires and the 1,4-BDT functionalized Zn_3P_2 nanowires.

Table 3. Linear fitting statistical results summary of the un-functionalized Zn_3P_2 nanowires and the 1,3-PDT functionalized Zn_3P_2 nanowires hydrogen evolution.

Functional group	Slope (Hydrogen production rate)		Statistics
	Value	Standard Error	R-Square
UF	30.36	1.31	0.98
BDT	1838.6	34.6	0.99

The un-functionalized Zn_3P_2 nanowires exhibits 30.36±1.31 μmol/g/hr hydrogen production rate in 4 hours test period, while the 1,4-BDT functionalized Zn_3P_2 nanowires yield 1838.6±34.6 μmol/g/hr hydrogen production rate, which agrees with the prediction made before. The hydrogen production rate the 1,4-BDT functionalized Zn_3P_2 nanowires is approximately 61 times higher than the hydrogen production rate of the un-functionalized Zn_3P_2 nanowires, besides the amount of hydrogen gases produced by the un-functionalized Zn_3P_2 nanowires could considered as insignificant production. The first half hour during photocatalytic hydrogen evolution reaction of the 1,4-BDT functionalized Zn_3P_2 nanowires, relatively small amounts of hydrogen gases were measured. This phenomenon could be explained as the initial photochemical activation[54] of the functionalized Zn_3P_2 nanowires. The photocatalytic hydrogen evolution reaction continues in a stable rate afterwards. The relatively low hydrogen production rate of un-functionalized Zn_3P_2 nanowires was due to the degradation with water that lose the nanowire structure. More importantly, the functional groups served as the electron transfer bridge between the bulk surface Zn_3P_2 nanowires and the reduction sites on the

functional molecules, thus would yield better hydrogen production rate. For the discussion of the functional molecules serve as the bridge of charge transfer, later sub-chapter will provide further explanations.

3.2 INVESTIGATION OF ELECTRON TRANSPORT THROUGH ALKANEDITHIOL FUNCTIONAL GROUPS

By functionalizing the Zn_3P_2 nanowires using organic alkanedithiol functional groups with different alkyl chain length, we are discussing the dependence between the alkyl chain length in alkanedithiol functional groups and the electron transfer rate. And the nanowire structure stability of the functionalized Zn_3P_2 nanowires were also investigated correlated to alkyl chain length in alkanedithiol functional groups. The purpose of investigate the electron transport mechanism through alkanedithiol functional groups is to synthesize the functionalized Zn_3P_2 nanowires and modified by organic alkanedithiol functional groups to obtain the surface modified Zn_3P_2 nanowires with high photochemical activity and structure stability. Since the Zn_3P_2 nanowires can be surface modified by variety of organic functional groups, it is critical to understand how electrons transfer between functional groups and the functionalized Zn_3P_2 nanowires, which would result in a thorough overall scope on how to choose the surface modification molecular to functionalize the Zn_3P_2 nanowires that occupies stable structure stability and high the photocatalytic activity.

Figure 10 shows a schematic of three functionalized Zn_3P_2 nanowires. In this section, the Zn_3P_2 nanowires were functionalized by 1,3-propanedithiol (noted as 1,3-

PDT), 1,4-butanedithiol (noted as 1,4-BDT) and 1,12-dodecanedithio (noted as 1,12-DDT) for comparison of the alkyl chain length in alkanedithiol functional groups. While for the

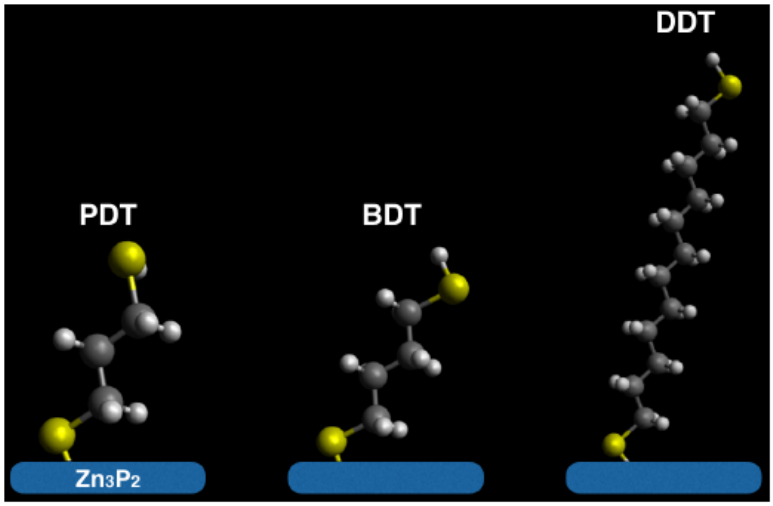

Fig. 10 Schematic of functionalized Zn_3P_2 nanowires with alkanedithiol groups (1,3-PDT, 1,4-BDT, 1,12-DDT)[55].

convenience view of the image, the molecular volume in space of those three functional molecules are not size proportional, besides the figure 10 only shows the most stable molecular structure of each of them and there are plenty of unstable structure of three molecular exist in each functionalized Zn_3P_2 nanowires samples. However the isomers are existing in each samples, the molecular volume in space are descending in the order of 1,12-DDT, 1,4-BDT and 1,3-PDT. The functional molecule with longer alkyl chain length not only occupies more volume in space, but also has stronger molecular interaction with each other. Therefore the molecule exclude with each other due to the repulsion force between the same molecules, and hence result different molecule surface

coverage for three different functionalized Zn_3P_2 nanowires. Because of the synthesize process are followed the same procedures before Zn_3P_2 nanowires functionalization, the un-functionalized nanowires are considered have the same morphology as well as the same zinc phosphate lattice before functionalization. Therefore reaction activate spot on the Zn_3P_2 nanowires for zinc atom are considered as the same, so in this case, 1,12-DDT functionalized Zn_3P_2 nanowires would have less surface coverage on the Zn_3P_2 nanowires bulk surface due to its higher volume size in space compare to Zn_3P_2/1,4-BDT and Zn_3P_2/1,3-PDT. In theory, the best to least molecular surface coverage of functionalized Zn_3P_2 nanowires are 1,3-PDT, 1,4-BDT and 1,12-DDT.

Photocatalytic hydrogen evolution experiments were preformed to test the hydrogen production rate of Zn_3P_2/1,3-PDT, Zn_3P_2/1,4-BDT and Zn_3P_2/1,12-DDT functionalized Zn_3P_2 nanowires.

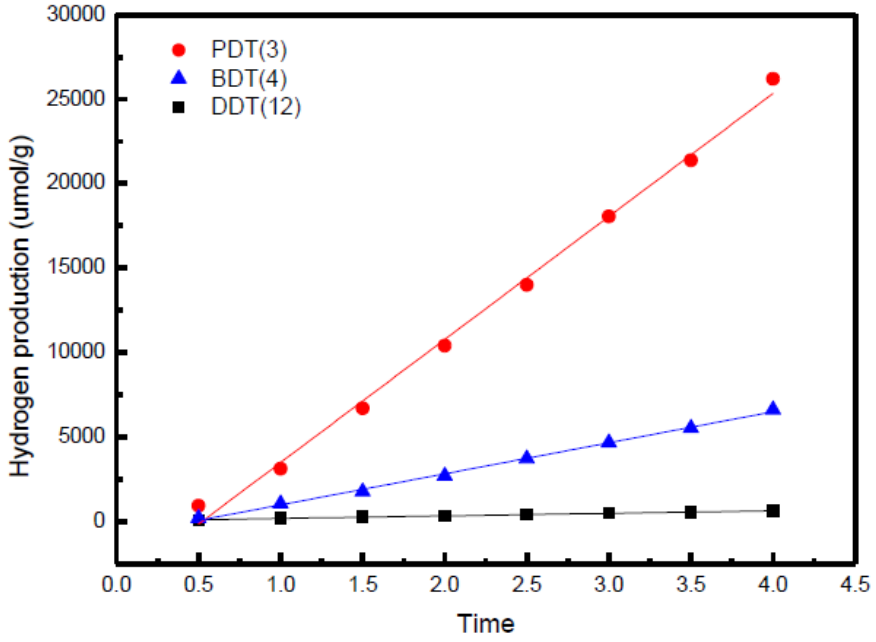

Fig. 11 Photocatalytic hydrogen evolution reaction results with alkanedithiol groups (1,3-PDT, 1,4-BDT, 1,12-DDT) photocatalysts[55].

Figure 11 shows that amount of hydrogen produced monotonically increased with time under visible light irradiation, from three different functionalized organic groups of the functionalized Zn_3P_2 nanowires, which suggests a stable and active photocatalytic reaction. In a 4-hour test period, Zn_3P_2/1,3-PDT exhibits the highest photocatalytic activity among all three different functional groups, followed by Zn_3P_2/1,4-BDT and Zn_3P_2/1,12-DDT respectively. Besides, the Zn_3P_2 nanowires functionalized by Zn_3P_2/1,12-DDT showed gentle photocatalytic activity that is hard to be observed in figure 11. For the first half hour, relatively small amounts of hydrogen gases were measured for all the three different functional groups[55]. This phenomenon is

the same as mentioned before as the initial photochemical activation of the functionalized Zn_3P_2 nanowires.

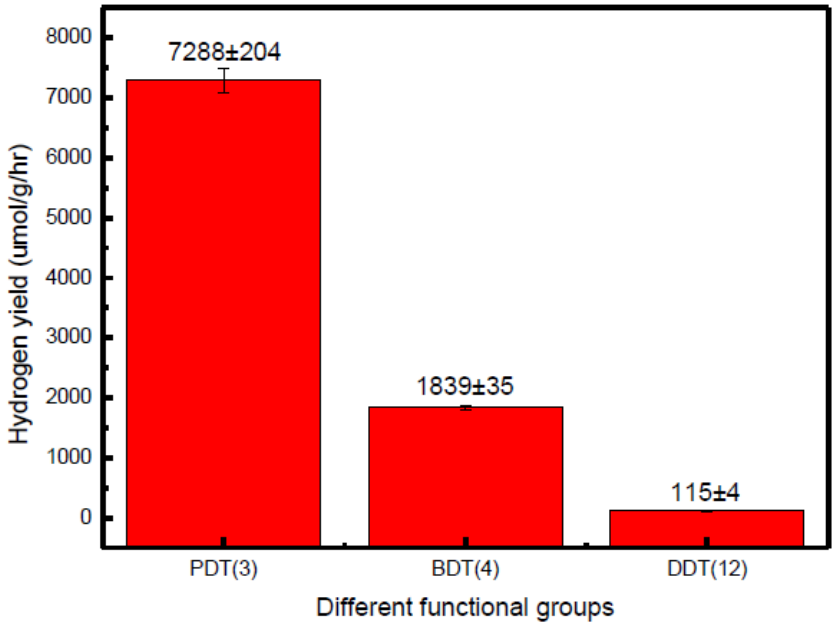

Fig. 12 Photocatalytic hydrogen evolution results of the dependence of different functional groups amount on photocatalytic activity for hydrogen evolution[55].

The hydrogen results in figure 12 shows that hydrogen production rates with 4 hours over Zn_3P_2/1,3-PDT, Zn3P2/1,4-BDT, and Zn_3P_2/1,12-DDT are 7288 ± 204, 1839 ± 35, and 155± 4 μmol/h/g, respectively. The hydrogen production rate of Zn_3P_2/1,3-PDT is approximately 4 times higher than that of Zn_3P_2/1,4-BDT and 63 times higher than that of Zn_3P_2/1,12-DDT respectively. The results indicate alkyl chain length have a significant impact on hydrogen production rate[55]. The mechanism of this behavior is further discussed below.

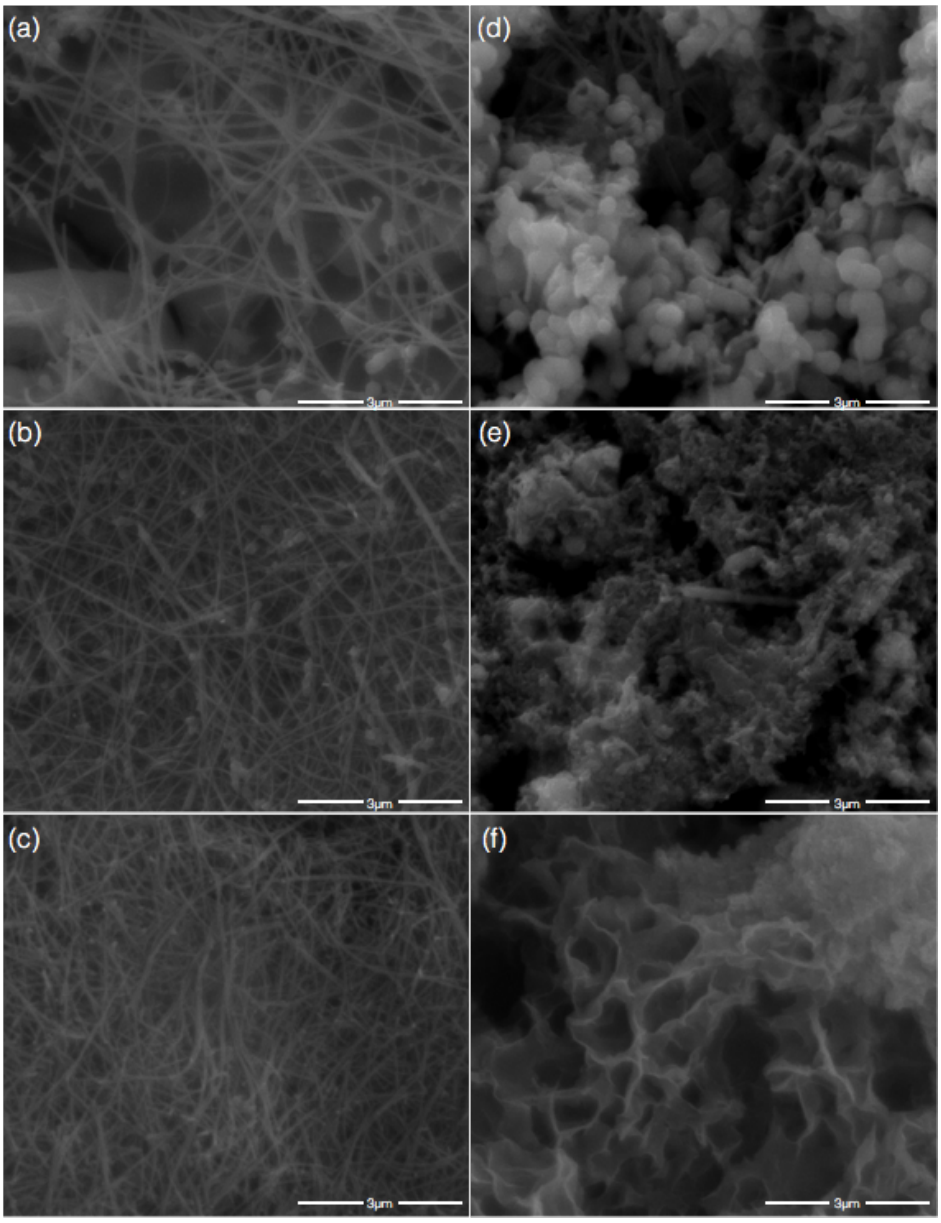

Fig. 13 SEM images of Zn_3P_2/1,3-PDT, Zn_3P_2/1,4-BDT, and Zn_3P_2/1,12-DDT respectively before (abc) and after (def) hydrogen evolution reaction[55].

Figure 13 shows the Scanning Electron Microscopy (SEM) images of the different functional groups before (abc) and after (def) hydrogen evolution reaction. As

shown in figure 13a, b and c, the functionalized Zn_3P_2 nanowires are kept in similar morphologies after the functionalization. Degradation of Zn_3P_2 nanowires occurs in all three functionalized groups after hydrogen evolution reaction. The degradation in morphologies transformed from nanowires to small particles combined with nanowires or degraded continuity surface, this photo-catalytic degradation could be explained that Zn_3P_2 reacting with water described by equation $Zn_3P_2 + 6H_2O \rightarrow 3(OH)_2 + 2PH_3$

As shown in figure 13, Zn_3P_2/1,3-PDT was found to be the most stable among three different functionalized groups, since it showed the least degradation of nanowire structure, while Zn_3P_2/1,4-BDT and Zn_3P_2/1,12-DDT appeared to lose the nanowire structure heavily. Zn_3P_2/1,12-DDT showed the most severe structure degradation as the nanowires structure have completely decomposed compare to the nanowire of Zn_3P_2/1,3-PDT and Zn_3P_2/1,4-BDT. This could be explained due to the different surface coverage of Zn_3P_2 nanowires. Functional groups with shorter alkyl chain length occupy less volume size in space; hence possess larger percentage of surface coverage of Zn_3P_2 nanowires. Thus the Zn atom that bonding with functional groups further prevent the diffusion of water onto Zn atom to form Zn hydroxide, and enhance the structure stability of Zn_3P_2 nanowires.

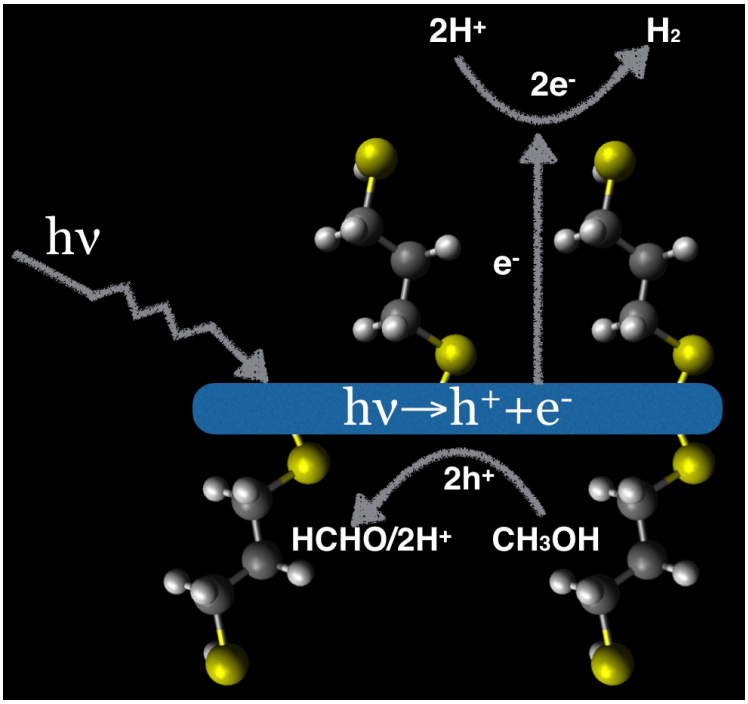

Fig. 14 Schematic of electrons and holes transfer and redox reactions on the functionalized Zn_3P_2 nanowires.

Figure 14 shows a possible hydrogen evolution mechanism and electron transfer direction on the functionalized Zn_3P_2 nanowires. The redox reaction on the functionalized Zn_3P_2 nanowires occurs at two different locations. Visible light is absorbed on the surface of the Zn_3P_2 bulk nanowires and generates holes and free electrons; the reaction occurs as follows $h\nu \rightarrow h^+ + e^-$. The photo-generated electrons is expected to transfer to the bond point of functional molecule, then they move along the organic functional group and end up at the end of the functional molecules, where the reaction of reduction of hydrogen ions occurs and leads to the formation of hydrogen, namely: $2H^+ + 2e^- \rightarrow H_2$. The photo-generated holes, on the other hand, stay on the

surface site of the bulk Zn_3P_2 nanowires, are not covered by organic functional groups, oxidizing methanol leading to the formation of formaldehyde and hydrogen ions: $2h^+ + CH_3OH \rightarrow HCHO + 2H^+$ [56, 57]. The surface of the Zn_3P_2 nanowires has a high possibility that it is not entirely covered by the organic functional groups since the formation defects occur during the synthesis process of the Zn_3P_2 nanowires as well as chemical vapor deposition process[58]. The rate of hydrogen production could be considered as the rate of electron transfer in this system. The more electrons undergo the reaction of reduction of hydrogen ions, the higher is the rate of formation of hydrogen.

One of the possible mechanisms to explain the electron transfer rate across alkyl chain is the tunneling effect from the Zn_3P_2 bulk nanowires to the end point of functional molecule. If an alkyl chain in a certain functional group is long, then the tunneling rate of that functional group is low[59]. Moreover, the rate of electron transfer (k_{ET}) on the functionalized Zn_3P_2 nanowires is exponentially related to the distance between photo-generated sites (donor) and the end point of functional molecule (acceptor); the relationship between the two is described by equation $k_{ET} = k_0 e^{-\beta d_{D,A}}$ (where k_0 is a pre-exponential factor; β is a structure-dependent attenuation factor that describes the decay of electronic coupling between donor and acceptor as the distance separating them increases; and $d_{D,A}$ is the distance separating the donor and acceptor)[60].

The electron can transport from the Zn_3P_2 nanowires bulk surface to the molecule by tunneling, and the rate of electron transfer also has influence on the electron transfer. Therefore the total reaction rate is limited by the tunneling rate and rate of electron transfer in the case of long alkyl chain. This explanation agrees with the experimental

results, as the alkyl chain length increases in alkanedithiol functional groups, the hydrogen production rate decreases dramatically when the alkyl chain length reaches 12. Similarly, the current density decreases as the distance between photo-generated sites and the end point of functional molecule increases. The exponential decrease in current is consistent with the electron transport rate [61, 62], described by equation $I = I_0 e^{-\beta d_{D,A}}$ Since the reduction current is proportional to the hydrogen reduction rate, then the alkyl chain length is dependent to hydrogen production rate as well. The shorter interatomic bonds favor the photo-generated electron transfer between the organic molecules and the Zn_3P_2 nanowires bulk surface. This observation also agrees with the lower tunneling rate of long alkyl chain, since the current in a tunneling is proportional to the probability of tunneling. In short, those two factors, electron transfer rate and current rate that are in corresponding with tunneling rate, both contribute to lower hydrogen production rate for longer alkyl chain in alkanedithiol functional groups.

The electron can transport from the Zn_3P_2 nanowires bulk surface to the organic molecule by tunneling, and the rate of electron transfer also has influence on the electron transfer. Therefore the total reaction rate is limited by the tunneling rate and rate of electron transfer in the case of long alkyl chain. This investigation can also serves the application of select suitable organic functional groups to surface modify Zn_3P_2 nanowires.

3.3 HYDROGEN PRODUCTION RATE COMPARISON BETWEEN THE FUNCTIONALIZED ZN_3P_2 NANOWIRES AND SYNTHESIZED Ag/Zn_3P_2 NANOCOMPOSITE.

The silver metal particles have influence on the electron transfer rate of the functionalized Zn_3P_2 nanowires bulk surface, the photo-generated electrons on the surface of the functionalized Zn_3P_2 nanowires transfered to the surface of silver particles, which change the electronic confinement on the functionalized Zn_3P_2 nanowires surface. Therefore mitigated the photo-generated hole and electron recombination process, as well as enhance the charge separation on the bulk functionalized Zn_3P_2 nanowires surface, therefore perform higher photochemical reaction activity compare to the functionalized Zn_3P_2 nanowires itself. The synthesized Ag/Zn_3P_2 nanocomposite photocatalysis can be considered as facilitate electron transfer from the functionalized Zn_3P_2 nanowires bulk surface to silver surface during the photochemical reactions. Moreover, the photo-generated electrons can be transfer by charge transfer process from the functionalized Zn_3P_2 nanowires bulk surface to functionalized alkyl chain groups through the zinc atoms. However abundant photo-generated electrons were still kept on the functionalized Zn_3P_2 nanowires bulk surface that cannot transfer through the molecules from the functionalized alkyl chain groups, the silver particles coated on the functionalized Zn_3P_2 nanowires bulk surface can serve as the reduction sites which the photo-generated electrons excited from the conduction band (CB) the functionalized Zn_3P_2 nanowires to the silver particle surface that react with hydrogen protons to

generate hydrogen gases, thus increase the hydrogen production rate of Ag/Zn_3P_2 nanocomposite photocatalysis.

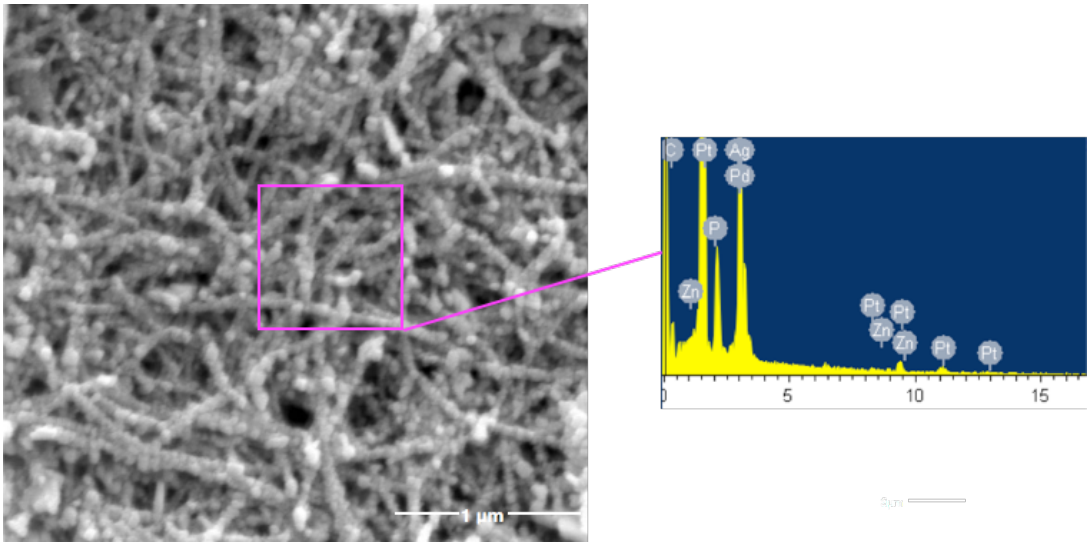

Fig. 15 SEM image and EDX element analysis of Ag/Zn_3P_2 (1,3-PDT functionalized) nanocomposite.

As shows in figure 15, the SEM image shows the synthesized Ag/Zn_3P_2 (1,3-PDT functionalized) nanocomposite are kept in similar nanowire morphologies like the functionalized Zn_3P_2 nanowires. In addition to the web-like nanowire structure, the synthesized Ag/Zn_3P_2 (1,3-PDT functionalized) nanocomposite have monolayer silver nanoparticles coated on the functionalized Zn_3P_2 nanowires. The diameter of the nanowires in the synthesized Ag/Zn_3P_2 (1,3-PDT functionalized) nanocomposite are around 40-60 nm, similar to the 1,3-PDT functionalized Zn_3P_2 nanowires and length of the nanowires approximately ~10µm, similar to the 1,3-PDT functionalized Zn_3P_2

nanowires as well. As shows in table 4, the diameter of the silver nanoparticles in the synthesized Ag/Zn_3P_2 (1,3-PDT functionalized) nanocomposite 77.48±10.13 nm.

Table 4. Diameter of synthesized Ag/Zn_3P_2 nanocomposite measurement.

Number	Area	Mean	Angle	Length	Actual value (nm)
1	13	129.12	-105.255	12.021	74.97
2	12	136.961	-68.199	11.424	71.25
3	13	142.848	-37.875	11.511	71.79
4	12	123.833	0	11	68.61
5	13	144.264	80.538	11.673	72.80
6	15	163.891	85.914	13.583	84.72
7	11	90.186	-60.945	10.296	64.22
8	14	226.413	-32.471	12.777	79.69
9	16	151.536	77.905	14.916	93.03
10	13	153.248	52.125	11.8	73.60
11	14	144.143	71.565	12.981	80.96
12	13	151.519	-74.745	11.885	74.13
13	11	155.829	-23.962	10.062	62.76
14	13	165.791	70.017	11.705	73.00
15	11	98.057	-53.13	10.308	64.29
16	15	156.765	45	14.142	88.20
17	16	157.531	23.199	15.232	95.00
18	15	157.489	-33.69	14.151	88.26
19	17	142.05	45	15.914	99.26

Table 4. Continued

Number	Area	Mean	Angle	Length	Actual value (nm)
20	15	183.079	26.565	13.647	85.12
21	12	125.797	-26.565	10.512	65.56
22	14	137.503	-94.399	13.086	81.62
23	15	135.233	-12.995	13.829	86.25
24	12	104.949	21.801	11.424	71.25
25	12	136.012	79.695	10.689	66.67
Mean					77.48
Standard deviation					10.13

The EDX results in indicated area shows the silver peak with 64.79% weight percent, indicate that the silver nitrate solution were successfully photo-deposited the silver nanoparticles on the functionalized Zn_3P_2 nanowires by UV light deposition method. The carbon peak was the carbon atom in the alkanedithiol functional groups, and Pt, Pd peak was deposited on the sample in order to do the SEM characterization, the Pt, Pd weight percentages were deducted from calculation to present the results clearly. Table 5 shows the element analysis of the indicated area from the SEM image in figure 15.

Table 5. Surface element analysis using EDX.

Element	Weight %
C	23.79
P	4.74
Zn	6.68
Ag	64.79
Total	100

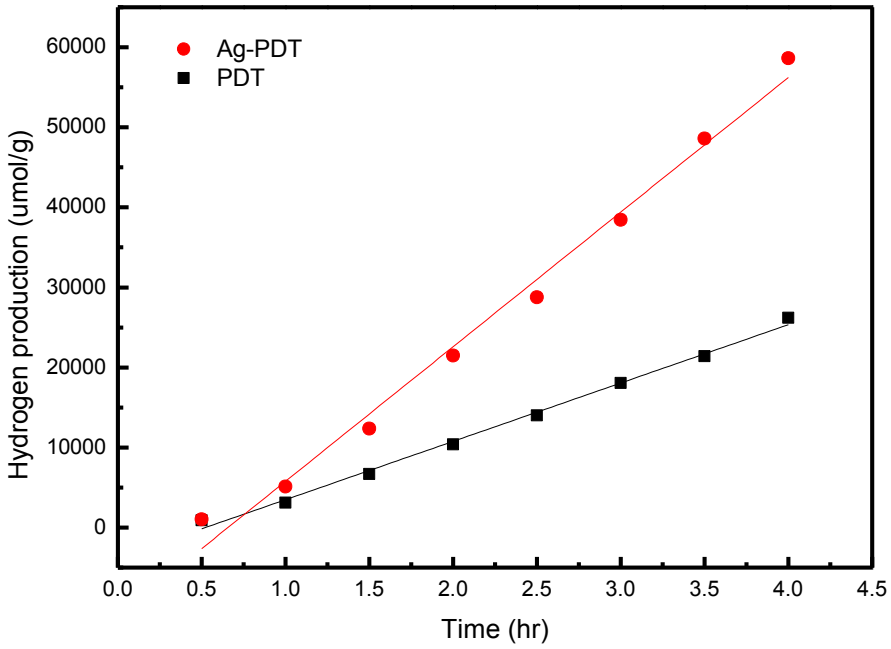

Fig. 16 Photocatalytic hydrogen evolution reaction results with Ag/Zn_3P_2 (1,3-PDT functionalized) nanocomposite and Zn_3P_2-1, 3-PDT.

Figure 16 shows the hydrogen production of the synthesized Ag/Zn_3P_2 (1,3-PDT functionalized) nanocomposite and the 1,3-PDT functionalized Zn_3P_2 nanowires increases monotonically with time during the photocatalytic hydrogen evolution, both the Ag/Zn_3P_2 (1,3-PDT functionalized) nanocomposite and the 1,3-PDT functionalized Zn_3P_2 nanowires exhibit stable hydrogen production in 4 hours time period. The Ag/Zn_3P_2 (1,3-PDT functionalized) nanocomposite exhibits higher photocatalytic activity than the photocatalytic activity of the 1,3-PDT functionalized Zn_3P_2 nanowires. Similarly to previous experiments, relatively small amounts of hydrogen gases were obtained because of the initial photochemical activation of the functionalized Zn_3P_2 nanowires for the first half hour in both experiments.

Table 6. Linear fitting statistical results summary of the Ag/Zn_3P_2 (1,3-PDT functionalized) nanocomposite and the 1,3-PDT functionalized Zn_3P_2 nanowires hydrogen evolution.

Functional group	Slope (Hydrogen production rate)		Statistics
	Value	Standard Error	R-Square
PDT	7288	204	0.98
Ag-PDT	16816	700	0.98

The photocatalytic hydrogen evolution results in figure 16 and table 6 shows that hydrogen production rates in 4 hours test period over the Ag/Zn_3P_2 (1,3-PDT functionalized) nanocomposite and the 1,3-PDT functionalized Zn_3P_2 nanowires are 16816±700 umol/g/h and 7288±204 umol/g/h, respectively. The hydrogen production rate of the Ag/Zn_3P_2 (1,3-PDT functionalized) nanocomposite is above 2.3 times higher than that of the1,3-PDT functionalized Zn_3P_2 nanowires. The results indicate that coating silver nanoparticles on the functionalized Zn_3P_2 nanowires have increased the hydrogen production rate for the functionalized Zn_3P_2 nanowires.

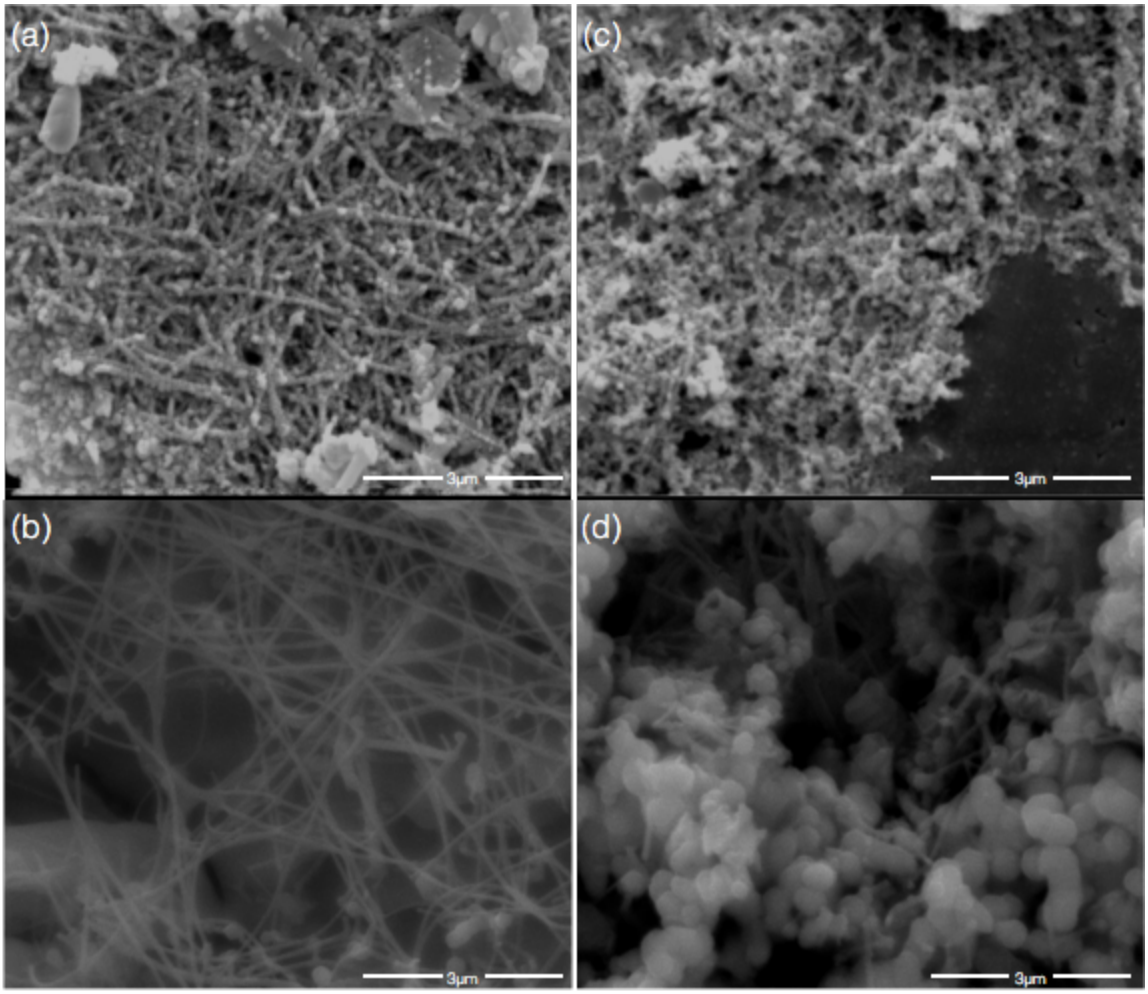

Fig. 17 SEM images of Ag/Zn_3P_2 (1,3-PDT functionalized) nanocomposite and Zn_3P_2-1,3-PDT respectively before (ab) and after (cd) hydrogen evolution reaction.

Figure 17 shows the SEM images of the Ag/Zn_3P_2 (1,3-PDT functionalized) nanocomposite and the 1,3-PDT functionalized Zn_3P_2 nanowires respectively before (ab) and after (cd) the 4 hours period photocatalytic hydrogen evolution. As shown in figure 17a the Ag/Zn_3P_2 (1,3-PDT functionalized) nanocomposite was kept in similar nanowire morphologies as the 1,3-PDT functionalized Zn_3P_2 nanowires. Degradation of the Ag/Zn_3P_2 (1,3-PDT functionalized) nanocomposite and the 1,3-PDT functionalized

Zn_3P_2 nanowires occurred after photocatalytic hydrogen evolution reaction. Those degradation caused by photocatalytic Zn_3P_2 nanowires react with water occurred more sever in the 1,3-PDT functionalized Zn_3P_2 nanowires than the Ag/Zn_3P_2 (1,3-PDT functionalized) nanocomposite. The nanowires structure degradation with water in morphologies transformed wire-structure into small particles combined with discontinuous shorter nanowires and degraded into discontinuity surface compare to the its structures before the photocatalytic hydrogen evolution reaction. However the Ag/Zn_3P_2 (1,3-PDT functionalized) nanocomposite maintained its majority nanocomposite morphology after the photocatalytic hydrogen evolution reaction, only part of its structure degraded after photocatalytic hydrogen evolution reaction as showed in figure 17c, compare to the 1,3-PDT functionalized Zn_3P_2 nanowires who lose the nanowire structure heavily. The SEM image of the Ag/Zn_3P_2 (1,3-PDT functionalized) nanocomposite after photocatalytic hydrogen evolution reaction still kept nanowire structure while the nanowires break into shorter pieces. The ability to against photocatalytic hydrogen evolution caused degradation is because of higher surface coverage of zinc atoms on nanowires of the Ag/Zn_3P_2 (1,3-PDT functionalized) nanocomposite that enhance the structure stability against the degradation, fewer zinc atoms exposing to the water in hydrogen evolution reaction, more stable the nanowire structure will be. The silver nanoparticles coated on the surface of functionalized Zn_3P_2 nanowires covered the zinc sites that not covered by the 1,3-PDT functional molecules, therefore maintain the same surface coverage as the 1,3-PDT functionalized Zn_3P_2 nanowires plus the addition silver nanoparticles coverage. The Ag/Zn_3P_2 (1,3-PDT

functionalized) nanocomposite preforms better stability in the hydrogen evolution reaction.

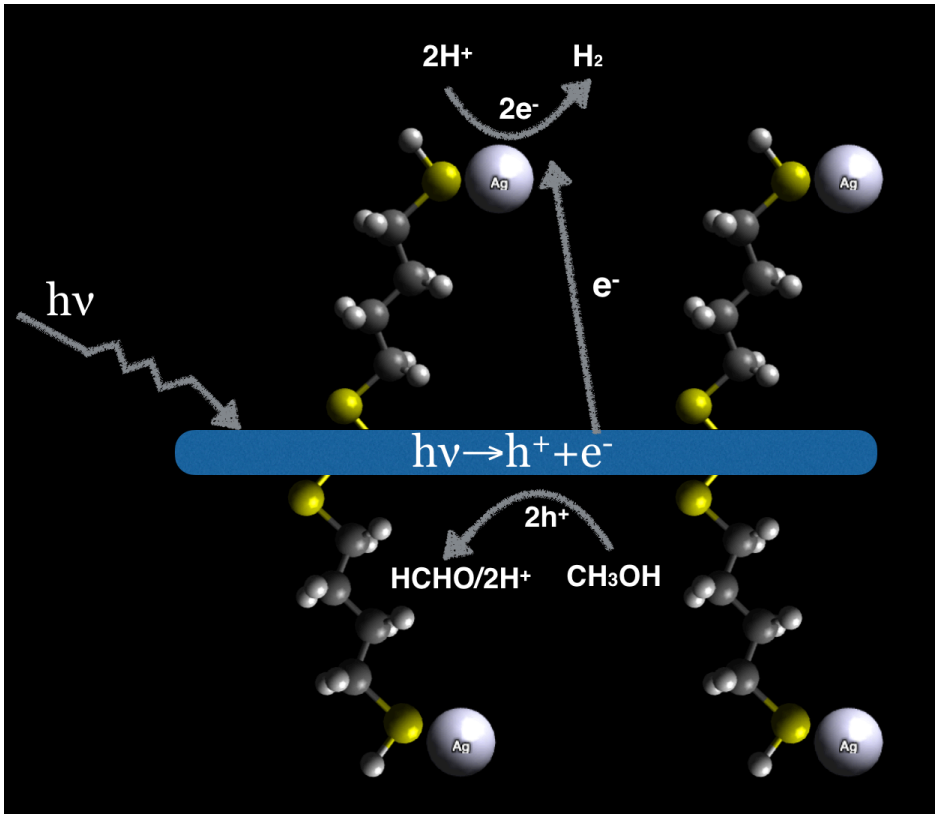

Fig. 18 Schematic of electrons and holes transfer and redox reactions on the synthesized Ag/ Zn_3P_2 (1,3-PDT functionalized) nanocomposite.

Figure 18 shows a possible photocatalytic hydrogen evolution reaction mechanism and electron transfer direction on the Ag/Zn_3P_2 (1,3-PDT functionalized) nanocomposite. The silver nanoparticles are attached to the sulfur atoms at the end of functional groups. The redox reaction on the Ag/Zn_3P_2 (1,3-PDT functionalized) nanocomposite occurs at two different types of reaction sites. Visible light absorption

occurred on the surface of the bulk Zn_3P_2 nanowires and generates holes and free electrons; the reaction occurs as follows $h\nu \rightarrow h^+ + e^-$. The photo-generated electrons are expected to transfer to the bridge molecule between functional molecule (1,3-PDT) and the Zn_3P_2 nanowires, then they move along with the organic functional group to the Ag atoms and end up reduced, where the reaction of reduction of hydrogen ions occurs and leads to the formation of hydrogen, namely: $2H^+ + 2e^- \rightarrow H_2$. The photo-generated electrons accumulated on the surface of silver nanoparticles, because the Fermi level of silver particles is lower than the Fermi level of the functionalized Zn_3P_2 nanowires . Because of the silver atoms, photo-generated electrons are more likely to transfer to the silver atoms passing through the organic molecules compare to the functionalized Zn_3P_2 nanowires without silver atoms, therefore enhanced the charge separation.

Meanwhile this facilitated transfer of electrons also mitigated the recombination process of electrons and holes, hence increase the photochemical activity for hydrogen production of Ag/Zn_3P_2 (1,3-PDT functionalized) nanocomposite compare to the photochemical activity of the 1,3-PDT functionalized Zn_3P_2 nanowires. This explanation agrees with the experimental results. The photo-generated holes stay on the surface site of the bulk Zn_3P_2 nanowires, transfer to the reaction sites that are not covered by the alkanedithiol functional groups and the silver nanoparticles, oxidizing methanol generate the formaldehyde and hydrogen ions: $2h^+ + CH_3OH \rightarrow HCHO + 2H^+$ [56, 57] .The surface of the Ag/Zn_3P_2 (1,3-PDT functionalized) nanocomposite has a high possibility that it is not entirely covered by the organic functional groups since the formation

defects occur during the synthesis process of the Zn_3P_2 nanowires as well as chemical vapor deposition process [58].

Based on the organic molecules that had attached on the Zn_3P_2 nanowires, the silver deposition are not entirely bonded with the organic molecules during the UV light deposition method due to the relatively low concentration of silver nitrate used in the synthesis process. The rate of hydrogen production could be considered as the rate of electron transfer in this system. The more electrons undergo the reaction of reduction of hydrogen ions, the higher is the rate of formation of hydrogen. Therefore by adding the silver nanoparticles on the functionalized Zn_3P_2 nanowires using UV light deposition method to synthesis the Ag/Zn_3P_2 (1,3-PDT functionalized) nanocomposite, could facilitate the charge transfer from Zn_3P_2 nanowires bulk surface to the silver nanoparticles, which in turns facilitate the hydrogen production rate.

CHAPTER IV

CONCLUSIONS AND FUTURE WORKS

In summary, it was shown the functionalized Zn_3P_2 nanowires exhibit better nanowire structure stability than the un-functionalized Zn_3P_2 nanowires against water-degradation for 10 days, and better photocatalytic activity as well. In the test of 1,3-PDT, 1,4-BDT and 1,12-DDT as the functional groups of Zn_3P_2 nanowires, as the alkyl chain decrease, the photocatalytic activity increases, due to the increased rate of electron transfer as well as vigorous tunneling effect, which ultimately enhanced the charge separation. The metal-doped Ag/ Zn_3P_2 nanowires nanocomposite exhibits higher photocatalytic activity than the functionalized Zn_3P_2 nanowires, because of lower the Fermi level of silver particles than the Fermi level of the functionalized Zn_3P_2 nanowires facilitates charge transfer and mitigated photo-generated electrons and holes recombination.

Further the dependence between the size of the Zn_3P_2 nanowires and photocatalytic hydrogen activity need to be investigated using SEM and UV-Vis. According to the Brus equation, band gap increases, which favors the hydrogen production, as the diameter of Zn_3P_2 nanowires decreases. In addition, Zn_3P_2 nanowires functionalized by shorter alkyl chain of the alkanedithiol (such as 1,2-EDT) need to be synthesized and investigated the photocatalytic hydrogen activity.

REFERENCES

1. Bhushan, M. and A. Catalano, *Polycrystalline Zn_3P_2 Schottky barrier solar cells.* Applied Physics Letters, 1981. 38(1): p. 39-41.
2. Zdanowicz, T., T. Rodziewicz, and M. Zabkowska-Waclawek, *Theoretical analysis of the optimum energy band gap of semiconductors for fabrication of solar cells for applications in higher latitudes locations.* Solar Energy Materials and Solar Cells, 2005. 87(1): p. 757-769.
3. Shockley, W. and H.J. Queisser, *Detailed balance limit of efficiency of p‐n junction solar cells.* Journal of applied physics, 1961. 32(3): p. 510-519.
4. Grätzel, M., *Photovoltaic and photoelectrochemical conversion of solar energy.* Philosophical Transactions of the Royal Society of London A: Mathematical, Physical and Engineering Sciences, 2007. 365(1853): p. 993-1005.
5. Li, B., et al., *Review of recent progress in solid-state dye-sensitized solar cells.* Solar Energy Materials and Solar Cells, 2006. 90(5): p. 549-573.
6. *International energy agency technical report, 2013 key world energy.* Statistics, 2013.
7. Sahaym, U. and M.G. Norton, *Advances in the application of nanotechnology in enabling a 'hydrogen economy'.* Journal of Materials Science, 2008. 43(16): p. 5395-5429.
8. Solomon, S., et al., *IPCC Fourth Assessment Report (AR4).* Retrieved, 2007. 4(13): p. 2011.

9. Martinot, E., *Renewables 2005: Global status report*. 2005: Worldwatch Institute Washington, DC.

10. Golosov, M., et al., *Optimal taxes on fossil fuel in general equilibrium.* Econometrica, 2014. 82(1): p. 41-88.

11. Scott, D., C.M. Hall, and S. Gössling, *A review of the IPCC Fifth Assessment and implications for tourism sector climate resilience and decarbonization.* Journal of Sustainable Tourism, 2016. 24(1): p. 8-30.

12. Dincer, I., *Green methods for hydrogen production.* International Journal of Hydrogen Energy, 2012. 37(2): p. 1954-1971.

13. Meng, N.I., et al. *Water electrolysis-a bridge between renewable resources and hydrogen*. in *Proceedings of the international hydrogen energy forum*. 2004.

14. Ni, M., et al., *A review and recent developments in photocatalytic water-splitting using TiO_2 for hydrogen production.* Renewable and Sustainable Energy Reviews, 2007. 11(3): p. 401-425.

15. Dincer, I. and C. Acar, *Review and evaluation of hydrogen production methods for better sustainability.* International Journal of Hydrogen Energy, 2015. 40(34): p. 11094-11111.

16. Nozik, A.J., *Photoelectrolysis of water using semiconducting TiO_2 crystals.* Nature, 1975. 257: p. 383-386.

17. Nozik, A.J., *Electrode materials for photoelectrochemical devices.* Journal of Crystal Growth, 1977. 39(1): p. 200-209.

18. Chojnowski, F., et al., *Hydrogen production by water photoelectrolysis with a powder semiconductor anode.* Chemical Physics Letters, 1981. 84(3): p. 555-559.

19. Bard, A.J., *Design of semiconductor photoelectrochemical systems for solar energy conversion.* The Journal of Physical Chemistry, 1982. 86(2): p. 172-177.

20. Aspnes, D.E. and A. Heller, *Photoelectrochemical hydrogen evolution and water photolyzing semiconductor suspensions: properties of platinum group metal catalyst-semiconductor contacts in air and in hydrogen.* The Journal of Physical Chemistry, 1983. 87(24): p. 4919-4929.

21. Getoff, N., *Photoelectrochemical and photocatalytic methods of hydrogen production: a short review.* International Journal of Hydrogen Energy, 1990. 15(6): p. 407-417.

22. Alstrum-Acevedo, J.H., M.K. Brennaman, and T.J. Meyer, *Chemical approaches to artificial photosynthesis. 2.* Inorganic Chemistry, 2005. 44(20): p. 6802-6827.

23. Domen, K., et al., *Photocatalytic decomposition of water vapour on an NiO–$SrTiO_3$ catalyst.* Journal of the Chemical Society, Chemical Communications, 1980(12): p. 543-544.

24. Sato, S. and J.M. White, *Photodecomposition of water over Pt/TiO_2 catalysts.* Chemical Physics Letters, 1980. 72(1): p. 83-86.

25. Ikeda, S., et al., *Overall water splitting on tungsten-based photocatalysts with defect pyrochlore structure.* Catalysis letters, 2004. 98(4): p. 229-233.

26. Zieliñska, B., E. Borowiak-Palen, and R.J. Kalenczuk, *Photocatalytic hydrogen generation over alkaline-earth titanates in the presence of electron donors.* International Journal of Hydrogen Energy, 2008. 33(7): p. 1797-1802.

27. Duonghong, D., E. Borgarello, and M. Graetzel, *Dynamics of light-induced water cleavage in colloidal systems.* Journal of the American Chemical Society, 1981. 103(16): p. 4685-4690.

28. Lee, S.-H., et al., *Significance of Hydrophilic Characters of Organic Dyes in Visible-Light Hydrogen Generation Based on TiO_2.* Organic letters, 2009. 12(3): p. 460-463.

29. Xiaobo, C., *Titanium dioxide nanomaterials and their energy applications.* Chinese Journal of Catalysis, 2009. 30(8): p. 839-851.

30. Anpo, M., et al., *The preparation and characterization of highly efficient titanium oxide-based photofunctional materials.* Annu. Rev. Mater. Res., 2005. 35: p. 1-27.

31. Chae, J., et al., *Hydrogen production from photo splitting of water using the Ga-incorporated TiO_2s prepared by a solvothermal method and their characteristics.* Bulletin of the Korean Chemical Society, 2009. 30(2): p. 302-308.

32. Shibata, M., et al., *Photocatalytic activities of layered titanium compounds and their derivatives for H_2 evolution from aqueous methanol solution.* Chemistry Letters, 1987(6): p. 1017-1018.

33. Domen, K., A. Kudo, and T. Onishi, *Mechanism of photocatalytic decomposition of water into H_2 and O_2 over NiO $SrTiO_3$.* Journal of Catalysis, 1986. 102(1): p. 92-98.

34. Kadowaki, H., et al., *Overall splitting of water by RuO_2-loaded $PbWO_4$ photocatalyst with $d^{10}s^2$-d^0 configuration.* The Journal of Physical Chemistry C, 2007. 111(1): p. 439-444.

35. Maeda, K., et al., *Photocatalytic overall water splitting on gallium nitride powder.* Bulletin of the Chemical Society of Japan, 2007. 80(5): p. 1004-1010.

36. Arai, N., et al., *Effects of divalent metal ion (Mg^{2+}, Zn^{2+} and Be^{2+}) doping on photocatalytic activity of ruthenium oxide-loaded gallium nitride for water splitting.* Catalysis Today, 2007. 129(3): p. 407-413.

37. Sato, J., et al., *RuO_2-loaded β-Ge_3N_4 as a non-oxide photocatalyst for overall water splitting.* Journal of the American Chemical Society, 2005. 127(12): p. 4150-4151.

38. Satsangi, V.R., et al., *Nanostructured hematite for photoelectrochemical generation of hydrogen.* International Journal of Hydrogen Energy, 2008. 33(1): p. 312-318.

39. Rajeshwar, K., *Materials aspects of photoelectrochemical energy conversion.* Journal of applied electrochemistry, 1985. 15(1): p. 1-22.

40. Walter, M.G., et al., *Solar water splitting cells.* Chemical reviews, 2010. 110(11): p. 6446-6473.

41. Chen, Z., H.N. Dinh, and E. Miller, *Photoelectrochemical water splitting.* SpringerBriefs in Energy, New York, 2013.

42. Hashim, A., *Advances in nanocomposite technology*. 2011.

43. van de Krol, R., Y. Liang, and J. Schoonman, *Solar hydrogen production with nanostructured metal oxides.* Journal of materials chemistry, 2008. 18(20): p. 2311.

44. Matsuoka, M., et al., *Photocatalysis for new energy production: recent advances in photocatalytic water splitting reactions for hydrogen production.* Catalysis Today, 2007. 122(1): p. 51-61.

45. Zong, X., et al., *Photocatalytic H2 evolution on MoS2/CdS catalysts under visible light irradiation.* The Journal of Physical Chemistry C, 2010. 114(4): p. 1963-1968.

46. Wadia, C., A.P. Alivisatos, and D.M. Kammen, *Materials availability expands the opportunity for large-scale photovoltaics deployment.* Environmental Science & Technology, 2009. 43(6): p. 2072-2077.

47. Kimball, G.M., et al., *Passivation of Zn3P2 substrates by aqueous chemical etching and air oxidation.* Journal of Applied Physics, 2012. 112(10): p. 106101.

48. Brockway, L., et al., *Large-scale synthesis and in situ functionalization of Zn3P2 and Zn_4Sb_3 nanowire powders.* Physical Chemistry Chemical Physics, 2013. 15(17): p. 6260-6267.

49. Ramos-Sanchez, G., et al., *Organic molecule-functionalized Zn_3P_2 nanowires for photochemical H_2 production: DFT and experimental analyses.* International Journal of Hydrogen Energy, 2014. 39(35): p. 19887-19898.

50. Ingram, D.B. and S. Linic, *Water splitting on composite plasmonic-metal/semiconductor photoelectrodes: evidence for selective plasmon-induced formation of charge carriers near the semiconductor surface.* Journal of the American Chemical Society, 2011. 133(14): p. 5202-5205.

51. Liu, Z., et al., *Plasmon resonant enhancement of photocatalytic water splitting under visible illumination.* Nano letters, 2011. 11(3): p. 1111-1116.

52. Kochuveedu, S.T., D.-P. Kim, and D.H. Kim, *Surface-plasmon-induced visible light photocatalytic activity of TiO_2 nanospheres decorated by Au nanoparticles with controlled configuration.* The Journal of Physical Chemistry C, 2012. 116(3): p. 2500-2506.

53. Alenzi, N., et al., *Photoelectrochemical hydrogen production from water/methanol decomposition using Ag/TiO_2 nanocomposite thin films.* international journal of hydrogen energy, 2010. 35(21): p. 11768-11775.

54. Yu, T.-H., et al., *$ZnFe_2O_4$ decorated CdS nanorods as a highly efficient, visible light responsive, photochemically stable, magnetically recyclable photocatalyst for hydrogen generation.* Nanoscale, 2013. 5(16): p. 7356-7360.

55. Li, H. and Z. Cheng, *Investigation of Electron Transport Through Alkanedithoil of Functionalized Zn_3P_2 Nanowires for Hydrogen Production.* Int J Nano Stud Technol S, 2016. 1: p. 1-5.

56. Burstein, G.T., et al., *Aspects of the anodic oxidation of methanol.* Catalysis Today, 1997. 38(4): p. 425-437.

57. Lu, X., et al., *Photoelectrochemical hydrogen production from biomass derivatives and water.* Chemical Society Reviews, 2014. 43(22): p. 7581-7593.

58. Love, J.C., et al., *Self-assembled monolayers of thiolates on metals as a form of nanotechnology.* Chemical reviews, 2005. 105(4): p. 1103-1170.

59. Tamura, J., et al., *Electrochemical reduction of CO_2 to ethylene glycol on imidazolium ion-terminated self-assembly monolayer-modified Au electrodes in an aqueous solution.* Physical Chemistry Chemical Physics, 2015. 17(39): p. 26072-26078.

60. Holmlin, R.E., et al., *Electron transport through thin organic films in metal-insulator-metal junctions based on self-assembled monolayers.* Journal of the American Chemical Society, 2001. 123(21): p. 5075-5085.

61. Barraud, A., P. Millie, and I. Yakimenko, *On the tunnel electron transport in metal/Langmuir–Blodgett film/metal systems.* The Journal of chemical physics, 1996. 105(16): p. 6972-6978.

62. Joachim, C., J.K. Gimzewski, and A. Aviram, *Electronics using hybrid-molecular and mono-molecular devices.* Nature, 2000. 408(6812): p. 541-548.